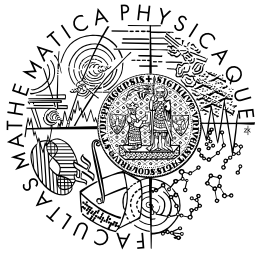

FACULTY
OF MATHEMATICS
AND PHYSICS
Charles University

MASTER THESIS

Benjamín Andreides

Modelling of precursors for electron-beam induced deposition

Department of Physics

Supervisor of the master thesis: Juraj Fedor
Study programme: Physics
Study branch: Biophysics and chemical physics

Prague 2021

I declare that I carried out this master thesis independently, and only with the cited sources, literature and other professional sources. It has not been used to obtain another or the same degree.

I understand that my work relates to the rights and obligations under the Act No. 121/2000 Sb., the Copyright Act, as amended, in particular the fact that the Charles University has the right to conclude a license agreement on the use of this work as a school work pursuant to Section 60 subsection 1 of the Copyright Act.

In ..... date ....

Author's signature

I would like to thank to Mgr. Juraj Fedor, PhD., who gave me an opportunity to work for him and to write this thesis, sending me to a secondment to MBN Research Center GmbH. to cowork with Professor Andrey Solov'yov and Alexey Verkhovtsev, PhD. (to which I am very thankful as well) and to learn advanced modelling and simulating of experiments by means of MBN Explorer and MBN Studio software packages.

Title: Modelling of precursors for electron-beam induced deposition

Author: Benjamín Andreides

Department: Department of Physics

Supervisor: Juraj Fedor, Heyrovsky Institute of Physical Chemistry

Abstract: FEBID (focused electron beam induced deposition) precursors are a subject of active research both in experimental and computer simulation manners. Their potential use in FEBID is strongly dependent on the completeness of the dissociation process caused by both primary and secondary electrons of the electron beam. This work focuses on exploration of dissociation process of iron pentacarbonyl cation by secondary electrons in i) vacuum ii) argon cluster environment and on possibility of utilizing argon cluster with an embedded gold particle as a non-covalently bonded precursor for FEBID. These systems will be inspected via means of the classical and reactive molecular dynamics using the rCHARMM force field.

Keywords: $Fe(CO)_5^+$ Argon Molecular dynamics Graphene Charmm Reactive Force Field MBN Explorer FEBID Clusters Dissociation Energy

Contents

1. Introduction into FEBID and precursor molecules

1.1 Focused Electron-Beam Induced Deposition

A fundamental purpose of FEBID (Focused Electron-Beam Induced Deposition) is to create 3-dimensional products of a nano-scaled volume by depositing atoms into substrate from a gaseous precursor floating above the substrate surface. In this approach, molecules of the gaseous precursor are destroyed through the interaction with the electron beam , while the usually metallic core of the molecule is being held on the surface. Although this approach seems to be promising, the practical examination of the process contains several difficulties depending on the properties of the used gaseous precursor.

There is a long history behind the idea of FEBID in relation with transmission electron microscopy (TEM) and scanning electron microscopy (SEM). Electrons strongly interact with the matter on the surface, thus creating errors in measurement in particular type of microscopy, but also revealing a new approach to the potential deposition and dissociation of a matter on such a surface via electron-molecule interactions. The idea behind FEBID is to fabricate structures on a scale that is comparable with the size of the electron beam, ideally with perfect purity and geometrical precision. Usual FEBID can be implemented in various experimental setups. The most fundamental parts of the system are always a source of electrons, a surface that we consider a work space (sample stage), and an injection system for organic gas, which brings the key material for the deposition to the surface. A visualization of a typical setup can be seen in Figure 1.1.

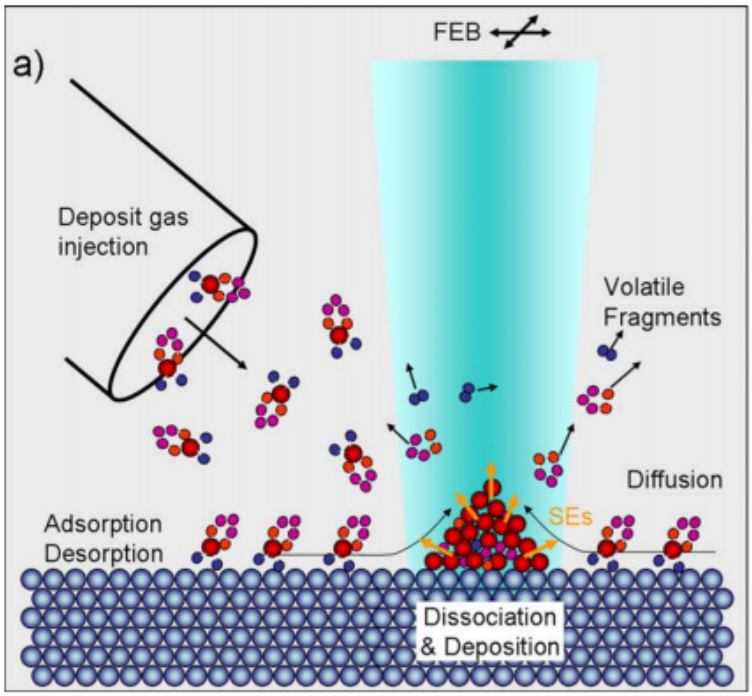

Figure 1.1: general setup of a FEBID system, from [1]

The organic gas used for FEBID is called a precursor and needs to fulfill several expectations, which will be discussed in the next section. Precursor molecule is injected into the sample stage, where it is dissociated in the focus of a high energy electron beam (keV). The core metal part of the precursor molecule is deposited on the surface. The residues of the dissociation process are pumped away. This process allows us to build a structure roughly resembling a 3D print structure (building the structure from bottom to top).

However, in this process, the dissociation tends to face several problems, which are always

specific for a particular precursor, and that is why precursors are being studied and developed in a manner that we can overcome these complications. Typical problems for the precursors involve imperfect dissociation, which means that in the deposited structure, there is always some impurity as an artifact of non ideal dissociation (for example in tungsten hexacarbonyl, we require all CO segments to be dissociated, so only a tungsten atom deposits onto the surface, but depending on the energy of the beam, there is always statistical a chance of a CO group deposited along with tungsten). In FEBID, interaction between a primary electron beam and a substrate necessarily results in creation of heat, and more importantly - in creation of secondary electrons in a small area around the primary electron impact [2]. Scheme of the production of various types of electrons can be found in the Figure 1.2. Energy of the secondary electrons is

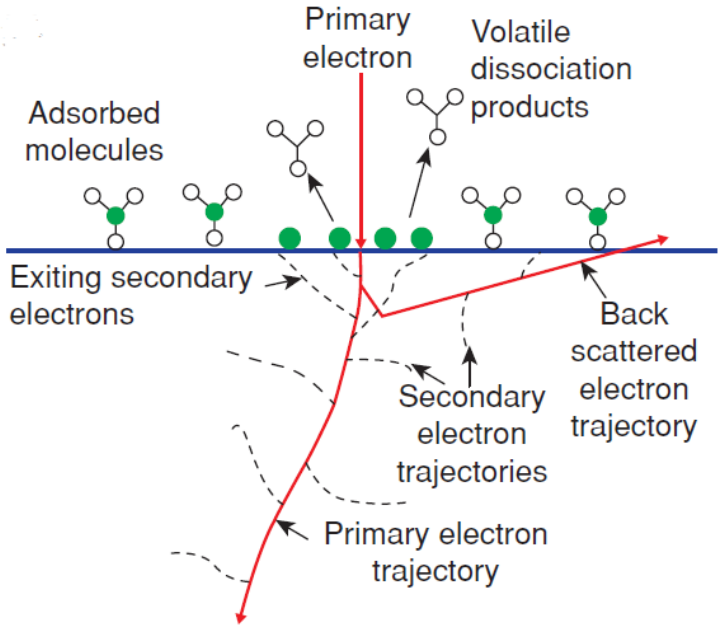

Figure 1.2: Types of electron produced in electron microscopy, from [2]

proportional to the primary electron beam energy, but generally equal to tens or thousands of electronvolts. Extent of primary versus secondary (and backscattered) electrons is still an open question that is being inspected, however secondary electrons follow much shorter mean free path before collision, since their energy is much smaller, therefore focus will be set on them, since their tendency to collide with a molecule is much higher.

1.2 Precursors for Electron-Beam Induced Deposition

1.2.1 Precursors in general

The precursors form a significant part of FEBID technology research and development. For deposition of metals, chemical vapor deposition precursors are usually applied [1]. The precursor choice must obey two general rules: they should be inert between themselves (not creating any chemical reactions without the presence of a beam), and also persist on the surface in the process of fabrication. Furthermore, there should exist a mechanism to desorb them from the substrate surface as well as the undesired fragments formed upon irradiation of precursors for the decomposition. These requirements are in conflict, meaning that an optimum of the process has to be searched.

The precursors are generally complexes consisting of central atoms and ligands. To achieve volatility, the molecule must be of zero charge, not too easy to polarize and not possess a strong dipole moment. To reach high sticking on a surface, this surface needs to be of opposite properties.

Let us now contemplate the ligands and center atoms. The simplest ligands are F, Cl, Br, I and H. The molecule can even be heteroleptic - when there are different ligands around the center atom. Quite commonly, molecules contain CO or PF_3 uncharged ligands. There are several factors to consider: the need to reduce the central ion for obtaining pure metal is a limiting factor, oppositely the electrostatic bond strength increases the stability of central ion complexes. Also, the presence of elements that easily polymerize like carbon is undesirable. Pure materials can be obtained if the electrons or ions initiate a chemical reaction but do not fragment the reaction products before the desorption of the final product. However, usually the deposition process is accompanied with unspecific multiple site fragmentation of adsorbed precursor molecules [1]. Better quality of the product can be obtained at relatively low electron densities and with precursors that dissociate easily, or that a chemical reaction such as an oxidation is initiated by electrons.

1.2.2 Iron pentacarbonyl

Often used precursors are metal carbonyls. The most usual compounds are $Ni(CO)_4$, $Fe(CO)_5$, $Fe_3(CO)_{12}$ and $W(CO)_6$. As known from quantum chemistry, the bond type between central atom and the uncharged ligands result in a configuration of the CO ligand being bonded to the center atom by the carbon atom. Due to the chemical properties of the carbonyls, there is no need for a redox reaction in order to liberate uncharged metals from the center. However, these types of bonds are relatively strong and dissociation of CO ligands from the metal center is not easy. At last, dissociation of all the CO ligands from the core is needed in order to achieve the optimal product. To make it even a bit more complicated, low energy electrons als induce dissociation of the CO group itself, which leads to liberation of O^+. This motivates the part of the thesis, which is dedicated to bringing a new insight into how the specific dissociation channels are proceeded in FEBID-related processes in the molecule of iron pentacarbonyl ($Fe(CO)_5$).

Not to forget to mention, why we began with iron pentacarbonyl in the first place, previous FEBID studies [11] & [14] showed that this particular molecule can achieve high purity of the resulting iron in the deposition process (more than 80%) without being chemically or physically processed afterwards. Also, compared to other metalorganic compounds, its toxicity is less severe. These studies used the FEBID process to create whole textures or shapes even with significant height and were able to measure its properties by the means of electron microscopy and mass spectroscopy . Different works mentioned in the work of Barth [11] already used this process for creating nanomagnets, which finds their application in computing and encoding binary operation [13] & [12], and characterized their deposits with magnetic force microscopy.

Although being studied generously, there still is a need for a better understanding of particular processes in the gas phase, particularly the dissociation process. Two specific mechanisms will be studied and compared in this work, formation of positive metal-containing ions via Electron Ionization (1.1) and Dissociative Ionization (1.2).

$$EI : M + e^- \rightarrow M^+ + 2e^- \tag{1.1}$$

$$DI : M + e^- \rightarrow (M - R)^+ + R + 2e^- \tag{1.2}$$

M stands for a target molecule, R is a free radical and $(M - R)^+$ is an arbitrary fragment ion. Many works report appearance energies (AEs) for particular reaction channels, however, there is quite a large scatter of the data (summarized in [3]). We will be taking the experimental data from the most recent study [3]. Since most, if not all, of the previous work is experimental, it is hard to judge if the suggested mechanisms are correctly assigned to particular reaction channels. DFT calculations in the work [3] are also useful, however they can't predict how the dissociation proceeds. That is why we will be using the means of reactive molecular dynamics explained in later chapters.

1.3 Gas phase experiments complementary to FEBID

To understand the most fundamental processes , we shall start with isolated molecules of iron pentacarbonyl in vacuum. For this purpose, let us briefly discuss the description of experimental and theoretical methods used in the work of Lacko [3]. They used crossed electron and molecular beam apparatus, where the vapor of $Fe(CO)_5$ was effused perpendicularly into beam of electrons (resolution of 0.25 eV) of a) fixed value of electronic energy at 70 eV, b) variable energy for monitoring abundance of created ions. From this, AEs for EI and DI were determined. As a comparison method, DFT calculations were done.

We can see in Figure 1.2, there are two possible forms of Fe-C bond. The first one between Fe and three CO groups is called equatorial and perpendicular to them are two CO groups with axial type of the bond. We expect even for them (can be seen in [3]) to behave differently upon electron interactions, but since there is no possibility to experimentally determine, which type of bond was dissociated, we can only consider simulation data to account. Lacko et al. [3], paid attention to the correct transition between symmetry states is given. However, the molecular dynamics may not necessarily lead to the ground state in each simulation. We rather discuss the statistical properties of the molecule and its interaction with electron, therefore no further focus on the actual quantum chemical state of the molecule is discussed (symmetry, excitation

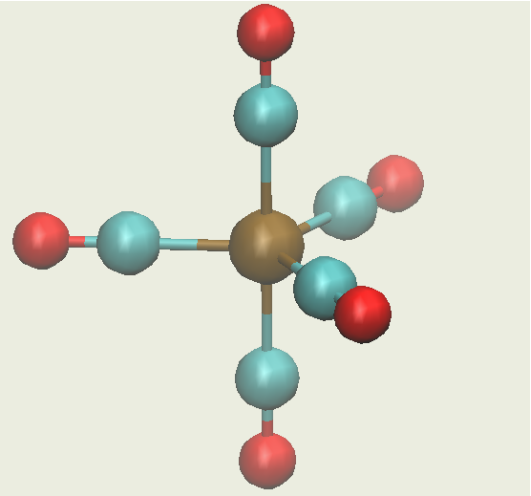

Figure 1.3: molecule of iron pentacarbonyl in its global minimum

m/z	Ion	Neutral	AE (eV)	AE – other authors (eV)					
				[3]	[4]	[5]	[6]	[7]	[8]
196	$Fe(CO)_5^+$		8.45	8.53	8.53	8.14	8.16	8.40	8.40
168	$Fe(CO)_4^+$	CO	9.00	9.30	10.00	8.34	8.73	9.17	9.30
140	$Fe(CO)_3^+$	2CO	10.28	10.08	10.30	9.80	10.01	10.04	10.10
124	$FeC(CO)_2^+$	2CO + O	17.66	18.20					
112	$Fe(CO)_2^+$	3CO	10.95	11.24	11.80	10.92	11.27	11.12	11.00
96	$FeC(CO)^+$	3CO + O	19.97	20.20					
84	$Fe(CO)^+$	4CO	12.82	13.18	14.00	12.90	13.39	13.76	14.00
72	FeO^+	4CO + C	22.95	22.50					
70	$Fe(CO)_3^{2+}$	2CO	23.57	24.00					
68	FeC^+	4CO + O	21.94	23.65			23.60		
56	Fe^+	5CO	14.65	15.51	16.10	14.70	15.31	15.99	16.20
48	$FeC(CO)^{2+}$	3CO + O	36.36						
42	$Fe(CO)^{2+}$	4CO	30.06	30.24	30.20				
28	CO^+	$Fe(CO)_4$	14.29						

Table 1.1: Appearance energies of various fragments of $Fe(CO)_5$ dissociation, from [3]

state, ...). The actual scope of this work is to compare the appearance energies given in Table 1.1. We will also determine the dissociation energy for stepwise removal of each CO group, as it is listed in Table 1.2. Lacko et al [3] measured their setup on a mass spectra analyzer, results of the spectra are depicted in Figure 1.4.

Positive ions	PBE0 BDE	Exp. BDE
T_d $^4A_2$ $(CO)_4Fe^+$-CO	1.05	0.55
C_{3v} $^4A_1$ $(CO)_3Fe^+$-CO	1.04	1.28
$D_{\infty h}$ $^4\sum_g$ $(CO)_2Fe^+$-CO	0.82	0.67
$C_{\infty v}$ $^4\sum$ $COFe^+$-CO	1.62	1.87
O_h $^6A_{1g}$ Fe^+-CO	1.71	1.82

Table 1.2: Dissociation energy for selected CO bonds from $Fe(CO)_5$ cation, from [3]

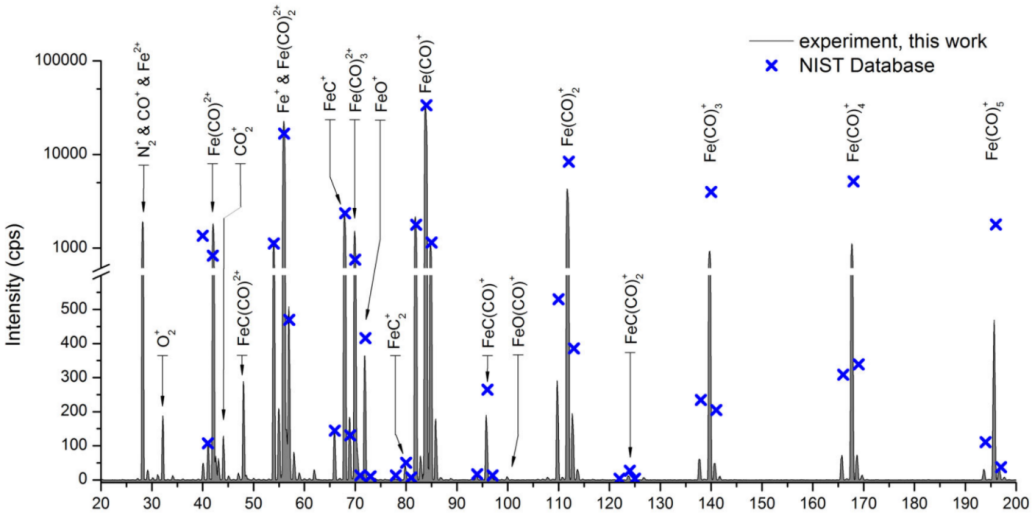

Figure 1.4: Mass spectra of $Fe(CO)_5$ molecule, from [3]

2. Introduction to Molecular Dynamics and Simulations

Since the rise of computer science in the middle of last century, physicists, chemists and biologists have been using computing power. Till today, a plethora of programs for molecular dynamics were developed, however, they are mostly not universal, and are assigned for specific types of problems. We talk about the near quantum mechanics scale of parametrization of atomic interactions, up to almost cellular organs. Also, from the view of parametrization of interatomic or intermolecular interactions, bio molecules, crystals in lattices, polymers - all require a slightly different approach in order to describe their physical properties.

In my thesis, I am using a highly universal MBN studio [15]. The main reason why this software is suitable for my work is that the experiments outlined in the previous chapter are at resolution, in which accompanying quantum chemistry is unnecessary and to some extent redundant. Other usual molecular mechanics software does not usually allow parametrization of chemical reactions - bonds breaking and their recreation. This phenomenon is however derived and conveniently approximated in what is called reactive CHARMM (rCHARMM) force field [21], which is implemented in the MBN Explorer. The bond dissociation and recreation of new complexes are exactly the issue I am going to investigate using molecular dynamics. Furthermore, one big positive aspect of this software is the ability to manually choose almost any existing and utilized potential, whether we are discussing pairwise, or many body potentials.

Since I am not using each of the possibilities provided by this software, but rather just some optimized options, I will discuss only them in the following sections.

2.0.1 Newtonian Dynamics & Verlet Algorithm

Basics of molecular dynamics are formulated via Newton's equations of motion. These equations, ignoring relativity and quantum character of particles are obeying equation:

$$m_i \vec{a_i} = m_i \frac{d^2 \vec{r_i}}{dt^2} = \vec{F_i} \tag{2.1}$$

for i = particles, where m is mass of an atom, $\vec{r}$ are its coordinates and $\vec{a}$ stands for its acceleration. For accommodating situations, where some of the positions of the molecule are rigidly fixed (for fastening up the simulation), Euler's equations are used. They are complementary to Newton's equations in this particular case of restricting the motion of several atoms of a molecule, since the molecule's motion is obeying Newton's equations in the center of mass, while also obeying Euler's equations in its rotation. The rotation is governed by the following equation:

$$\frac{d\vec{L_\alpha}}{dt} = \vec{T_\alpha} \tag{2.2}$$

for α = rigid atoms in the system, where $\vec{L_\alpha}$ is the total angular momentum of a rigid molecule, $\vec{T_\alpha}$ is the total torque. However, this equation would be correct only in the case of working in an inertial system. Since the frame in which the coordinate axes are aligned along the principal axes of rotation of the molecule and $\vec{L_\alpha}$ possesses its simplest form is not inertial, we need to to define two Cartesian coordinate systems - lab frame (x,y,z) and molecular frame (x´,y´,z´). Now, after the coordinate system is redefined, we yield a new equation for rotation along the center of mass in equation:

$$\frac{d\vec{L_\alpha}}{dt} = \frac{d\vec{L'_\alpha}}{dt} + \vec{\omega'} x \vec{L'} \alpha. \tag{2.3}$$

Now, let us write following transformations:

$$\vec{T'_\alpha} = (T_{\alpha'_x}, T_{\alpha'_y}, T_{\alpha'_z}) \tag{2.4}$$

$$\vec{\omega'_\alpha} = (\omega_{\alpha'_x}, \omega_{\alpha'_y}, \omega_{\alpha'_z}) \tag{2.5}$$

and

$$\vec{L'_\alpha} = (I_{\alpha'_{x'x'}}\omega_{\alpha'_x}, I_{\alpha'_{y'y'}}\omega_{\alpha'_y}, I_{\alpha'_{z'z'}}\omega_{\alpha'_z}) \tag{2.6}$$

where $I_{\alpha'_{q'q'}}$ are principal moments of inertia of a rigid molecule. This transformation leads us into equation for Torque in the molecular frame as follows:

$$T_{\alpha_{x'}} = I_{\alpha'_{x'x'}}\dot{\omega}_{\alpha'_x} - (I_{\alpha_{y'y'}} - I_{\alpha_{z'z'}})\omega_{\alpha'_y}\omega_{\alpha'_z}, \tag{2.7}$$

which is the final equation for a rotation of a rigid molecule, as described in MBN Explorer book [17].

Now that we have our equations for motion, which are derived without any approximations in the process, we now need to introduce the basics of molecular **dynamics** - the motion itself. For this, I am using Velocity Verlet Integrator [18]. A paper dedicated to analysis of how does the MBN Explorer software work [16] describes the implementation of the Velocity Verlet Integrator in the following way: let $\vec{r}$(t),$\vec{v}$(t) and $\vec{a}$(t) be coordinates, velocity and acceleration of the center of mass of a rigid molecule, or a single atom. Also, in the case of a rigid molecule, let $\vec{\omega'}$(t) and $\vec{T'}$(t) be its angular velocity and torque in molecular frame, while $\mathbf{q}$(t) be the quaternion that describes the orientation of the molecular frame compared to lab frame. The algorithm then does the following procedure.

I) calculate velocities for all of the particles in the system at the middle of the time step $\Delta t/2$:

$$\vec{v}(t + \frac{\Delta t}{2}) = \vec{v}(t) + \vec{a}(t)\frac{\Delta t}{2} \tag{2.8}$$

II) Update the position for the center of mass of all particles:

$$\vec{r}(t + \Delta t) = \vec{r}(t) + \vec{v}(t + \frac{\Delta t}{2})\Delta t = \vec{r}(t) + \vec{v}(t)\Delta t + \vec{a}(t)\frac{\Delta t^2}{2} \tag{2.9}$$

III) Now it updates forces acting on all of the particles in the system and torques acting on all the rigid molecules and then accelerations for all the particles:

$$\vec{a}(t + \Delta t) = \vec{F}(t + \Delta t)/M_\alpha \tag{2.10}$$

IV) Update velocities for all the particles in the system:

$$\vec{v}(t + \Delta t) = \vec{v}(t + \frac{\Delta t}{2}) + \vec{a}(t + \Delta t)\frac{\Delta t}{2} \tag{2.11}$$

V) Calculate the angular acceleration in the molecular frame for the rigid molecules in the system:

$$\dot{\omega}_{x'}(t) = \frac{1}{I_{x'x'}}[T_{x'}(t) + (I_{y'y'} - I_{z'z'})\omega_{y'}(t)\omega_{z'}(t)] \tag{2.12}$$

VI) Calculate the first and second time derivatives of quaternions describing the orientation of all of the rigid molecules in the system:

$$\dot{\mathbf{q}}(t) = \frac{1}{2}\mathbf{q}(t) * \vec{\omega'}(t) \tag{2.13}$$

$$\ddot{\mathbf{q}}(t) = \frac{1}{2}(\dot{\mathbf{q}}(t) * \vec{\omega'}(t) + \mathbf{q}(t) * \frac{d\vec{\omega'}}{dt}(t)), \tag{2.14}$$

where $*$ denotes quaternion multiplication by a vector.
VII) Update the orientation described by quaternions for all of the rigid molecules in the system:

$$\mathbf{q}(t + \Delta t) = \mathbf{q}(t) + \dot{\mathbf{q}}(t)\Delta t + \ddot{\mathbf{q}}(t)\frac{\Delta t^2}{2} \tag{2.15}$$

VIII) Calculate the angular velocity for all the rigid molecules at the middle of the time step $\Delta t/2$:

$$\vec{\omega'}(t + \frac{\Delta t}{2}) = \vec{\omega'}(t) + \frac{d\vec{\omega'}}{dt}(t))\frac{\Delta t}{2} \tag{2.16}$$

IX) Calculate the torque-dependent part of the angular acceleration for all the rigid molecules:

$$\dot{\omega_i}^{(0)}(t+\Delta t) = \frac{T_i(t+\Delta t)}{I_{ii}} \tag{2.17}$$

X) Calculate the zeroth-order correction to the angular velocity:

$$(\vec{\omega'})^{(0)}(t+\Delta t) = \vec{\omega'}(t+\frac{\Delta t}{2}) + (\frac{d\vec{\omega'}}{dt}(t))^{(0)}(t+\Delta t)\frac{\Delta t}{2} \tag{2.18}$$

XI) Calculate the first-order correction to the angular acceleration:

$$\dot{\omega_{x'}}^{(1)}(t+\Delta t) = \frac{1}{I_{x'x'}}[(I_{y'y'} - I_{z'z'})\omega_{y'}^{(0)}(t+\Delta t)\omega_{z'}^{(0)}(t+\Delta t)] \tag{2.19}$$

XII) Calculate the first-order correction to the angular velocity:

$$(\vec{\omega'})^{(1)}(t+\Delta t) = (\vec{\omega'})^{(0)}(t+\Delta t) + (\frac{d\vec{\omega'}}{dt}(t))^{(1)}(t+\Delta t)\frac{\Delta t}{2} \tag{2.20}$$

XIII) Calculate the second-order correction to the angular acceleration:

$$\dot{\omega_{x'}}^{(2)}(t+\Delta t) = \frac{1}{I_{x'x'}}[(I_{y'y'} - I_{z'z'})\omega_{y'}^{(1)}(t+\Delta t)\omega_{z'}^{(1)}(t+\Delta t)] \tag{2.21}$$

XIV) Update angular velocities:

$$(\vec{\omega'})^{(2)}(t+\Delta t) = (\vec{\omega'})^{(0)}(t+\Delta t) + (\frac{d\vec{\omega'}}{dt}(t))^{(2)}(t+\Delta t)\frac{\Delta t}{2} \tag{2.22}$$

From the series of introduced equations, relevant equations (Newton's or Euler's or both) are applied to each particle of the system, so that $\vec{r}(t+\Delta t)$, $\vec{v}(t+\Delta t)$, $\vec{a}(t+\Delta t)$, $(\vec{\omega'})^{(2)}(t+\Delta t) = \vec{\omega'}(t+\Delta t)$, $\vec{T'}(t+\Delta t)$ and $\mathbf{q}$(t+Δt) are computed each step.

However, this numerical approach, which divides the whole simulation into small steps, never yields the analytical results. It can only round the results around certain accuracy, at which we consider the simulation valid. Specifically, we speak about orders of global error, which results from both non-analytical solutions of the dynamics of the system, and number representation in computers. If we optimize these two parameters (using a correct time step), we receive a global error for positions of particles in order of O(Δt^2) while the global error for velocities is O(Δt^2) as well. Further analysis of errors done by Velocity Verlet algorithm, is provided in literature [19].

2.0.2 Langevin Thermostat

One of the very important features in molecular dynamics is Thermostat. From the equipartition theorem we already know [20] that the particles operating in every degree of freedom possess the same kinetic energy $E_k = \frac{1}{2}k_bT$. This concludes a direct effect for the distribution of kinetic energy (temperature fluctuations), which has the form

$$p(\Delta T)\Delta T = \frac{1}{\sqrt{2\pi\sigma}} exp(-\frac{(T-T_0)^2}{2\sigma^2}), \tag{2.23}$$

where $\sigma^2 = 2T_0^2/N_{fr}$ and N_{fr} is the number of degrees of freedom in the system. To maintain this distribution, while also following the desired temperature, Langevin updated both the Newton's and Euler's equations in the following manner:

$$m_i\vec{a_i} = m_i\frac{d^2\vec{r_i}}{dt^2} = \vec{F_i} - \frac{1}{\tau_d}m_i\vec{v_i} + \sqrt{\frac{2k_bT_0mi}{\tau_d}}\vec{R_i}(t) \tag{2.24}$$

Here we can see, that more terms are added to the Newton's equation, k_bT is the thermal energy in the system, τ_d is the viscous damping time and $\mathbf{R}_i(t)$ is a delta-correlated stationary Gaussian process with zero mean, so that:

$$< \mathbf{R}_i(t) >= 0 \tag{2.25}$$

$$< \mathbf{R}_i(t)\mathbf{R}_i(t') >= \delta(t-t'), \tag{2.26}$$

where sharp brackets denote time averaging. Interpretation of Langevin thermostat can be imagined as friction force and noise accompanying the movement of the particles. Similarly for Euler equation we get:

$$T_\alpha = T_{0_\alpha} - \frac{1}{\tau_d} I_\alpha \omega_\alpha + \sqrt{\frac{2k_b T_0 I_\alpha}{\tau_d}} \vec{R'}_\alpha(t), \tag{2.27}$$

where T_{0_α} is the torque acting on the rigid molecule, ω'_α is the angular velocity, I'_α is the diagonalized tensor of moments of inertia and $\vec{R}_\alpha$ is a delta correlated stationary Gaussian process, again.

2.0.3 Interatomic Potentials

In this section, I will discuss the basics of the potentials, which are usually present in most of the present simulations. Most fundamental potentials can be divided into two groups - pairwise and many body potentials.

Part of the whole energy described by pairwise potentials obeys a general equation

$$U_{pw} = \sum_{i=1}^{N} \sum_{j<i}^{N} U(r_{ij}), \tag{2.28}$$

where we sum over all pairs of atoms in the system. Usually the most two important potentials are Coulomb and Lennard-Jones potentials. Coulomb potential is described by

$$U(r_{ij}) = \frac{q_i q_j}{\epsilon r_{ij}} \tag{2.29}$$

where q_i and q_j are the charges of atoms and ϵ is the dielectric constant and Lennard-Jones potential is described by:

$$U(r_{ij}) = \epsilon[(\frac{r_{min}}{r_{ij}})^{12} - 2(\frac{r_{min}}{r_{ij}})^{6}], \tag{2.30}$$

where r_{min} is the distance of potential minimum between these two atoms and ϵ is the strength of the potential.

Now lets introduce at least one many body potential. In my work, I am utilising Brenner potential for carbon layers, which is derived from the general form of many body potential

$$U_{mb} = \sum_{i=1}^{N} U_i(\vec{r_i}) \tag{2.31}$$

into

$$U_{br} = \frac{D_e}{2(S-1)} \sum_i \sum_{i \neq j} f_{cut}(r_{ij})[e^{-\sqrt{2S}\beta(r_{ij}-R_0)} - SB_{ij}e^{-\sqrt{\frac{2}{S}}\beta(r_{ij}-R_0)}], \tag{2.32}$$

where $f_{cut}(r_{ij})$ is the cutoff function that excludes the interactions from beyond neighbour atoms, which is assigned the following way:

$$f_{cut}(r_{ij}) = \begin{cases} 1, r_{ij} \leq R_1 \\ 0.5(1 + cos(\frac{r_{ij}-R_1}{R_2-R_1}\pi)), R_1 < r_{ij} < R_2 \\ 0, r_{ij} \geq R_2. \end{cases}$$

Also, the β_{ij} is the bond-order term, defined as:

$$\beta_{ij} = [1 + \sum_{k \neq i,j} f_{cut}(r_{ik}) G(\Theta_{ijk})]^{-\delta} \tag{2.33}$$

and the $G(\Theta_{ijk})$ defined as:

$$G(\Theta_{ijk}) = a_0[1 + \frac{c_0}{d_0}^2 - \frac{c_0^2}{d_0^2 + (1 + cos(\Theta_{ijk})}] \tag{2.34}$$

where the angle Θ_{ijk} is the angle between bonds formed by pairs of atoms with indices i,j and i,k.

2.0.4 Boundary Conditions

Since we cannot operate with infinitely large systems, but rather in a finite cubic space of a certain volume, we need to state, what happens if a particle moves to the border of this virtual cube. In my work, I used Periodic Boundary Conditions. This decision comes from the fact that I am using a rather small molecular system, which should not end up in any meaningless collision in case that the particles "reappear" from other directions.

The principle behind Periodic Boundary Conditions is that particles that would collide into the wall of a virtual cube will continue in its movement and appear from the opposite wall with its velocity and acceleration unchanged. At a large scale of boundary conditions, this means only that the particle does not disappear, energy of the system doesn't change and until the volume of the molecule is reasonably smaller than the volume of the cubic boundaries, it shouldn't end up in interaction that is unwilling for processes of certain kind.

2.1 Reactive Molecular Dynamics

As mentioned before, for the convenience of my work I am introducing reactive CHARMM (rCHARMM) force field [21]. The major difference comes from the ability to rupture and recreate chemical bonds. Take for instance classical harmonic approximation of covalent bonds:

$$U_{ij}^{bond} = k_{ij}^{b}(r_{ij} - r_0)^2. \tag{2.35}$$

This approximation predicts the behaviour of the covalent bond as a "spring" between two atoms, which is accurate for small deformations from the minimal distance from equilibrium r_0 (k_{ij} is the bond strength and r_{ij} is the actual distance between atoms). Reactive force field takes instead the more accurate Morse potential, which reads as:

$$U_m(r_{ij}) = D_{ij}[e^{-2\beta_{ij}(r_{ij}-r_0)} - 2e^{-\beta_{ij}(r_{ij}-r_0)}], \tag{2.36}$$

where D_{ij} is the bond dissociation energy and β_{ij} is the steepness of the potential and is equal to:

$$\beta_{ij} = \sqrt{k_{ij}^{b}/D_{ij}} \tag{2.37}$$

This way we can see that the Morse potential can be derived from standard harmonic approximation built into the standard (non-reactive) CHARMM force field, and another expansion for its Reactive update is a cutoff distance. We can assume that at distances $r_{ij} \gg r_0$ the atoms start to interact much stronger via Lennard-Jones potential, as can be seen from the following figure. Therefore, setting up a cutoff distance at a reasonable value and replacing it

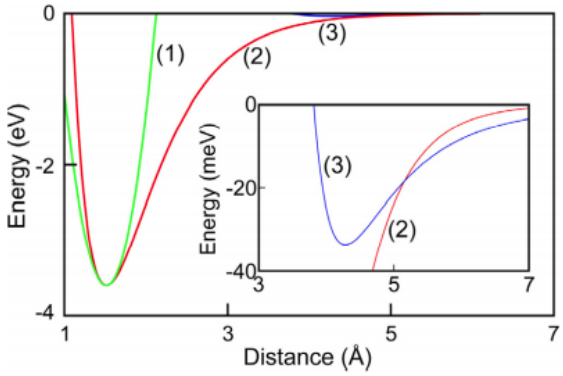

Figure 2.1: transition from strong covalent bond (green stands for harmonic approximation, red for morse potential and blue for Lennard-Jones potential), taken from [21]

with Lennard-Jones potential is allowed without a loss of inconvenient precision.

Now comes the question, what to do with other attributes of covalent bonds described by general CHARMM. It contains angle, dihedral angle and improper dihedral parts to fully

represent the behavior of chemical bonds. One step per another, angle potential between three atoms with indices ij and jk reads as:

$$U_{ijk}^{angle} = k_{ijk}^{a}(\theta_{ijk} - \theta_0)^2. \tag{2.38}$$

In the reactive force field there is provided a different parametrization:

$$U_{ijk}^{cos} = 2k_{ijk}^{a}[1 - cos(\theta_{ijk} - \theta_0)]. \tag{2.39}$$

For larger deformations, this new parametrization describes an energy threshold which is more suitable for modeling of bond cleavage. It makes sense that if the bond is ruptured by the means of increasing distance, the angle part of potential breaks as well. Therefore a special cutoff function $\rho(r_{ij})$ is defined the following way:

$$\rho(r_{ij}) = 1/2(1 - tanh[\beta_{ij}(r_{ij} - r_{ij}*)], \tag{2.40}$$

where $r_{ij}* = (R_{ij}^{vdW} + r_0)/2$. In figure 2.2 we can see the fundamental look of the cutoff function. Following the same pattern as with bond potential, this function operates between the equilibrium value r_0 up to the van der Waals contact value R_{ij}^{vdW}. Final bond potential is

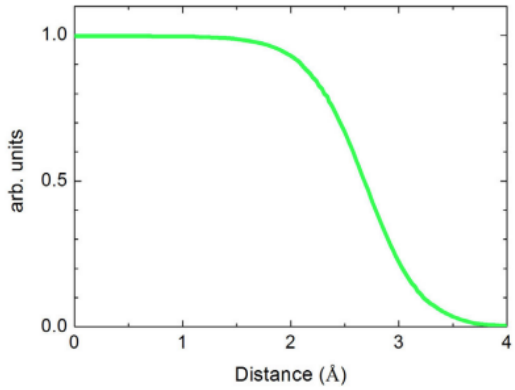

Figure 2.2: Cutoff function introduced for Reactive CharMM taken from [21]

then parametrized as:

$$U_{ijk}^{angle,react} = \rho(r_{ij})\rho(r_{jk})U_{ijk}^{cos}. \tag{2.41}$$

Similar procedure applies also to the dihedral part of the potential, which in harmonic approximation gives a formula:

$$U_{ijkl}^{dihedral} = k_{ijkl}^{d}[1 + cos(n_{ijkl}\chi_{ijkl} - \delta_{ijkl})], \tag{2.42}$$

where k_{ijkl}^{d}, n_{ijkl}, δ_{ijkl} are parameters of the potential, and χ_{ijkl} is the dihedral angle between the planes formed by atoms i,j,k and j,k,l. The rupture of a dihedral interaction between atoms i,j,k,l should count with three bonds between atoms that contribute to this interaction. So it follows that dihedral potential reads as:

$$U_{ijkl}^{dihedral,react} = \rho(r_{ij})\rho(r_{jk})\rho(r_{kl})U_{ijkl}^{dihedral} \tag{2.43}$$

Now the rupture of bonds is almost finished, the only remaining part is the redistribution of charges. The charge redistribution obeys the following conditions: i) a general one applicable to any molecule ii) a special one where charges within molecules are redistributed according to the known electronic configurations. The general mechanism is activated on rupture or formation of covalent bonds. In the case of a rupture, two new fragments have likely non-compensated, non-integer charges. Total charge of each new fragment is therefore rounded to the closest integer value and the charge difference is transferred from one fragment to another. Then this difference is redistributed evenly among all atoms of the fragments. Upon the formation of a new bond, the charge is redistributed inside the new molecule in order to lower the values of partial charges preserving the initial sum of charges.

Now for the final part, let us discuss the formation of new bonds. In MBN Explorer [16], after the rupture of a chemical bond between two atoms, a new list for them is created which

defines them as chemically active atoms. Only atoms in this list can participate in chemical reactions. For each atom in this list, the number of possible molecular bonds is determined by its valence. Therefore the input file also needs to include a list of valences for atoms involved. A chemical bond is created if the following criteria have been met: i) input parameters for this interaction are defined (equilibrium length, bond formation energy), ii) atoms are modeled as bound through Morse potential and iii) the distance between these two atoms is less than the predefined cutoff radius.

2.2 Model building and Simulations

Three different setups are analyzed and discussed in terms of evaluation of potential precursors. First, we will take a look on the dissociative ionization of iron pentacarbonyl itself. On this molecule, I will be applying the same methodology that was used in the article of de Vera et al. [22]. After validating this methodology on the $Fe(CO)_5{}^+$ and comparing it with the experimental results given by Lacko [3], I will expand this methodology to a system of $Fe(CO)_5$ deposited on argon cluster with parameters equal to conditions described in the work of Lengyel [23]. As the last part, a more speculative idea for the deposition using argon cluster as non-covalent ligands will be simulated and tested by the means of molecular dynamics. Instead of using specific organometalic presursor, I will inspect whether there is any possibility to use van der Waals bound rare gas cluster to deposit a dedicated metal element for FEBID-like purposes.

2.2.1 Iron pentacarbonyl cation

Let us now get from the basic introduction to the specific arrangement of the simulation. It is expected, that this particular molecule has its internal energy equal to the distribution of kinetic energies of Boltzmann distribution at 300 K temperature (before the dissociation process). In addition, a convenient time for the dissociation process is in a scale of nanoseconds (up to 1 μs), so I set the running time of my simulations to 100 ns. Now that the conditions given by the "real world" are designed, we can arrange the simulation properties accordingly.

First, we created a single $Fe(CO)_5$ cation and optimized it using rCHARMM force field with parameters derived from DFT calculations. Taking into account the fact that this molecule creates two different types of bonds between iron and carbon, it is necessary to distinguish between them, assigning CF1 notation for the 2 ligands in the "z" axis of the molecule, also known as axial type of bonds and CF2 notation for the 3 ligands in the perpendicular "xy" plane - for the equatorial type of bonds. DFT calculations were performed using the same methodology as was previously used in the work of De Vera [22] on a B3LYP functional with LanL2DZ basis set, resulting in dissociation energy of 37.549 kcal/mol (1.630 eV) for Fe-CF1 type of bond and 26.261 kcal/mol (1.138 eV) of energy for Fe-CF2 type of bond and the bond between carbon and oxygen has a dissociation energy of 230.700 kcal/mol (10.004 eV). After creating this molecule in MBN Explorer, a thermalization was done using Langevin thermostat at 300 K in 100x100x100 Å box with periodic boundary conditions for 1 nanosecond (with 1 femtosecond timestep). This procedure was performed 4 times and from these 4 simulations I took 10 different timestamps at which the molecule was equilibrated for each simulation, creating 400 statistically meaningful input files to work with. After this, two separate mechanism of energy deposition have been considered.

In the first mechanism, the energy is distributed between all degrees of freedom of the molecule. Therefore it will be always mentioned as **excess energy statistically distributed among atoms**.This means that I added various amounts of energies (10,20,30,...,250 kcal/mol or 0.434,....,10.84 eV) equally into kinetic energies of each component of the velocity for every atom, such that the vectors of the velocities were just re-scaled by the fraction of the energy distributed. For this process, box of 200x200x200 Å with periodic boundary conditions was utilized, and the whole simulation took 100 nanoseconds with timestep of 0.1 femtosecond and no thermostat.

The second mechanism is related to energy deposition into a specific part of the system; in this case, into a particular covalent bond. In future, I will be refering to that as **excess energy given into Fe-C bond**. We regard $Fe(CO)_4$ to be a heavy subsystem compared to a single CO ligand, therefore in a small approximation, the whole energy was distributed to the CO ligand, again in form of kinetic energy with step of 13,25,38,... up to 600 kcal/mol (0.564,1.128,...26.02 eV) with 13 kcal/mol (0.564 eV) step at smaller values of energy and 25 kcal/mol (1.128 eV) at the areas beyond 250 kcal/mol (10.84 eV). These simulations were executed in 200x200x200 Å periodic box in duration of 25 nanoseconds with 0.1 femtosecond timestep.

Important to mention, focus of this work is on dissociative ionization, therefore a single charged $Fe(CO)_5^+$ ion as a starting point was considered. This means that the excessive deposited energy will be given with respect to the ionization threshold of the molecule (which is 8.45 eV according to work of Lacko [3]).

For the first mechanism, 1120 simulations were executed, while for the second mechanism, 1532 simulations were performed.

2.2.2 Iron pentacarbonyl cation on argon cluster

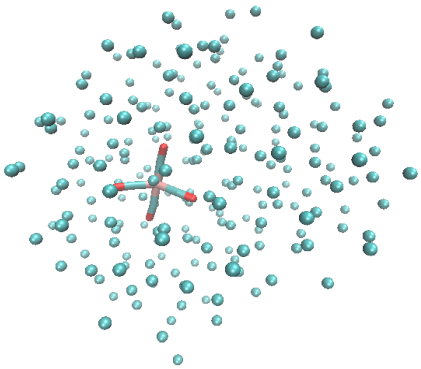

Figure 2.3: Iron pentacarbonyl cation on argon cluster

This system is the first step towards mimicking the real-world FEBID deposition. There, the iron pentacarbonyl is not freely flowing in space during the deposition process (in the perimeter of the primary beam), but rather sitting on a surface of either a substrate, or a previously deposited iron-based metal. It is thus incorrect to assume that the dissociation process will remain the same because of the effects introduced by decreased or diminished degrees of freedom for movement of certain CO groups of the molecule. Therefore it is convenient to embed this molecule into a medium that also reduces the movement of certain parts of the molecule, such that we can observe similar effect as it is observed while performing a real FEBID process. Lengyel et al. [23] used large argon clusters in order to mimic the elementary environment and its influence on the $Fe(CO)_5$ dissociative ionization. Here I model this system computationally.

What I did with iron pentacarbonyl on an argon cluster is very similar to what was done in previous section. First, there was a need to determine a correct geometry of the target $Fe(CO)_5$ cluster system. Experimentally [23], the mixed clusters were produced by pick-up of gas phase $Fe(CO)_5$ on pure argon clusters. In simulation, single molecule of $Fe(CO)_5$ collided with an argon cluster of typical volume and temperature ($\sim$ 300 atoms and 40 K) with a velocity of 490 m/s, which corresponds to an average velocity of the cluster in the experiment of Lengyel [23]. After this collision, a thermal loss of argon atoms from the cluster while the $Fe(CO)_5$ molecule gets embedded into the cluster is expected. The thermal relaxation is expected to happen down to the cluster-forming temperature of 40 K. This embedded molecule in cluster is expected to be a starting point for the dissociation simulation. From this point, we enter a similar situation that was discussed in previous section, deposing various amounts of energies into specific bonds of the $Fe(CO)_5$ molecule - 0,50,...,500 kcal/mol (0,2.17,....,21.7 eV) with 50 kcal/mol (2.17 eV) step at the whole grid of energy and 10 kcal/mol (0.434 eV) at the areas within the expected region of appearance energies from the experiment of Lengyel [23]. Excessive deposited energy is given with respect to the ionization threshold of Lengyel's work (8.3 eV). After all of this steps were proceeded, 2850 simulations ran in a length of 25 ps, using rCHARMM force field, periodic box of 200x200x200 Å and 0.1 femtosecond timestep.

2.2.3 Argon cluster as a potential ligand

As a last part of the simulations, a somewhat exotic situation was analyzed. Since the deposition of a certain metal through excitation and dissociation of the metalorganic precursor is accompanied by relics that we want to avoid (imperfection of the dissociation leading to an impure product), I tried to computationally explore the possibility to use a single metal-atom embedded into an argon cluster as a precursor. Such system, relying on its van der Waals interactions to hold the metal atom inside the cluster, would carry the metal to the substrate but (hopefully) prevent its deposition. The electron beam would evaporate the argon atoms away, while holding the metal atom only in the position of the beam. In theory, this would make the deposition process much easier due to lack of inconvenient chemical processes that occur in typical depositions with metalorganic precursors. However, since non-bonding interactions are much weaker than bonding interactions, the goal is to inspect which parameters (landing

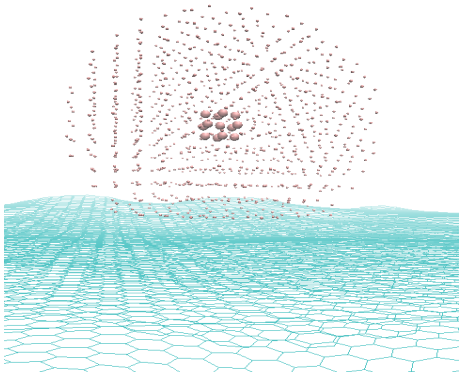

Figure 2.4: Possible appearance of Argon cluster with gold particle inside

velocity, temperature of the surface, volume of the cluster) are suitable for such idea. I will be answering this in the results section. There are several tasks that need to be resolved. All of them have one common denominator - the metal particle must not remain on the surface, but it should rather float on a layer of argon minimally for a duration of the simulation.

Let us discuss the parameters that need to be optimized to such event being successfully executable. The cluster should be small enough to allow multiple atoms of a metal, in our case gold, to be in the radius of an electron beam. Yet, it should be large enough to absorb the impact to the surface, not allowing the gold to drop into the surface of the substrate. Velocity of this system approaching to the surface should be small enough to allow the cluster not to scatter from the surface, while still being set realistically. Temperature of the surface should be low enough, so the cluster does not evaporate from the surface, which is around 40 K in the case of pure argon cluster. The last issue that needs to be taken into account are van der Waals attractive forces, which will drag the approaching cluster into the surface of the substrate, even without giving the gold-argon cluster any primary approaching velocity.

Since these parameters have too many options to vary, only few of the combinations of the arrangements will be mentioned in the results section. Van der Waals attractive forces tend to add approximately 1 Kelvin of temperature due to attractive motion they create when the gold argon cluster is in the vicinity of the surface. Therefore we can expect that the temperature, at which the cluster remains in its crystal form around the gold core will still be around the mentioned 40 K. Remaining question is whether the substrate is allowed to be of higher (e.g. room) temperature, and whether the approaching velocity can reach typical velocities of the injected argon cluster.

To finish the chapter of modelling strategy, tables of parameters are included on this page.

atom 1	atom 2	bond strength	equilibrium length	dissociation energy	cutoff
		kcal/mol/$Å^2$	Å	kcal/mol	Å
FE	CF1	114.99	1.882	37.549	5.0
FE	CF2	114.99	1.896	26.261	5.0
CF1	O	500.00	1.131	230.700	5.0
CF2	O	500.00	1.131	230.700	5.0

Table 2.1: Table of parameters for rCharMM force field computed for this work

atom 1	atom 2	ϵ	$r_m$in	cutoff	from
		kcal/mol	Å	Å	
C	C	0.003	3.89	10	[17]
Au	C	0.033	3.49	10	[26]
Au	Ar	0.065	3.34	10	[29]
Ar	Ar	0.010	3.82	10	[29]
Ar	C	0.005	3.79	10	[27]

Table 2.2: Table of parameters for non-covalent force field from various works

Additionally to the parameters in tables 2.1 and 2.2, Brenner potential for carbon was used in creation of a graphene substrate. Parameters for this potential can be seen in the Figure 2.3.

Brenner potential	
Parameter	Value
R_1 (Å)	1.70
R_2 (Å)	2.00
D_e (eV)	6.325
S	1.29
λ ($Å^{-1}$)	1.5
R_0 (Å)	1.315
δ	0.80469
a_0	0.011304
c_0	19
d_0	2.5

Table 2.3: Parameters for construction of graphene layer using Brenner potential, from [17]

3. Comparison of the results, simulations versus experiments

3.1 Dissociation of iron pentacarbonyl cation

Let me begin with qualities that can be compared with the work of Lacko [3] - appearance energies of the single charged fragments.

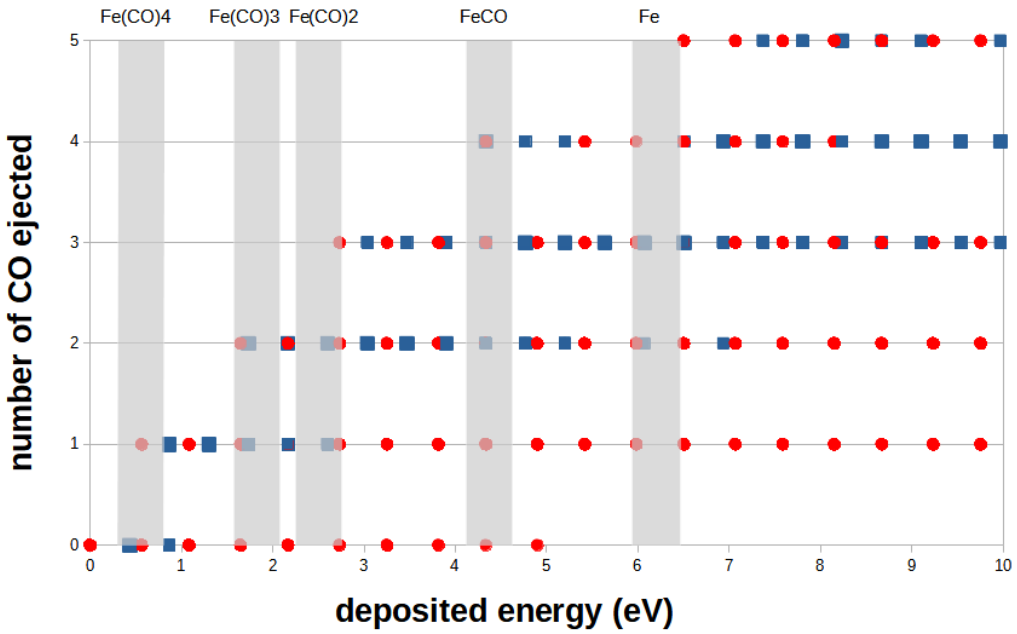

Figure 3.1: Appearance energies of various $Fe(CO)_n{}^+$ ions, excess energy statistically distributed among atoms is shown with blue squares, excess energy given into Fe-C bond is marked with red circles and the experimental data of Lacko cations are grey areas - mean values with the uncertainties

Let us describe, what can be seen in Figure 3.1. It shows which cations ($Fe(CO)_5{}^+$ minus given number of CO ligands) were detected in the simulation as a function of deposited energy. Ionized $Fe(CO)_5$ molecule has a threshold for its ionization (for a Fe-C bond) between 8.14 and 8.53 eV as it was measured in previous works [3, 5, 4]. This portion of energy (8.45 eV) is thus omitted from the appearance energies inspected by Lacko. This means that the x-axis of the Figure 3.1. corresponds to the internal energy of the ion (on top of its molecule's ionization potential). I deposited the internal energy via two different ways, as described in the previous section - excess energy statistically distributed among atoms, and excess energy given into Fe-C bond. As we can see, both ways contribute to the appearance energies and are in a good agreement with the experiment. This means that these two ways are equally important in this dissociation process. However, my goal is not to only agree with the experiment, but to give also an insight into the distributions of individual created ions depending on the deposited energy. For this purpose, let us see the next two figures.

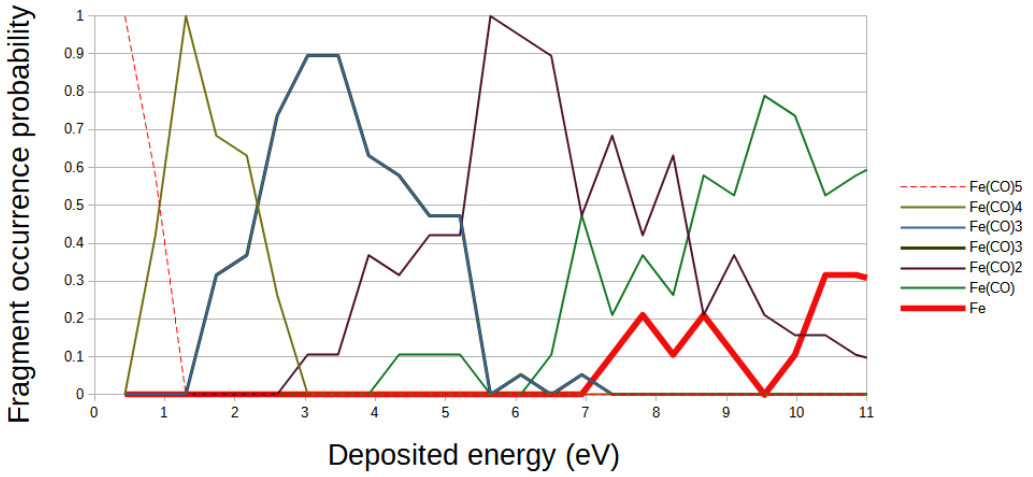

Figure 3.2: Abundance of various $Fe(CO)_n{}^+$ ions depending on the deposited energy created via excess energy statistically distributed among atoms

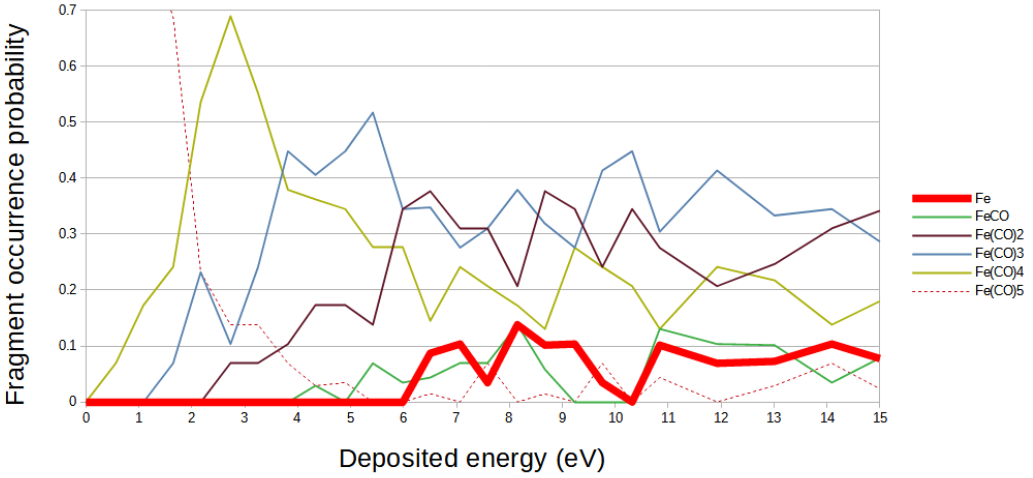

Figure 3.3: Abundance of various $Fe(CO)_n{}^+$ ions depending on the deposited energy created via excess energy given into Fe-C bond

Figures 3.2 and 3.3 bring us another interesting result. They show abundance of various $Fe(CO)_n{}^+$ ions as a function of deposited energy. The system has much more distinguished regions of occurrence of particular -nCO fragments of the molecule when the excess energy is statistically distributed among atoms, than when the excess energy is given into Fe-C bond. Giving the energy into Fe-C bond affects directly only one specific bond at the beginning and all the other bonds are broken just as a result of energy transfer via intramolecular vibrational redistribution (IVR). This certainly broadens the distribution of an occurrence of the multiple bonds breaking process depending on energy, which creates a strong overlap, as we can see in Figure 3.3. In FEBID, we generally would like to obtain more separated regions of the occurrence of particular ions, since it would mean that technically you can adjust the setup to enhance the desired channel the most. Lastly, in Figures 3.2 and 3.3 we can see that the processes, where the final desired Fe^+ fragment is created are not as frequent as the processes that lead to other fragments, which is not very desired.

Now let us discuss the further results. Although in reality non-controllable, analysis of the differences of the dissociation processes after deposing energy between iron and CF1/CF2 bonds can bring some insights into differences between these scenarios. Results can be seen in Figures 3.4 (a) to (f). As we can see in Figure 3.4, there are no significant regions, where one of the channel is dominant, closed, or have any other significant statistical relevance, although there

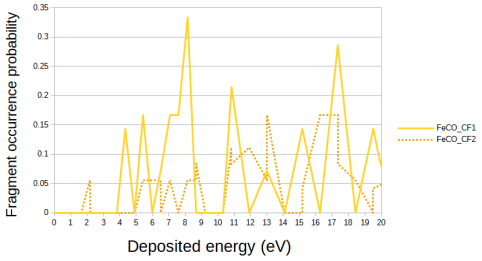

(a) FeCO

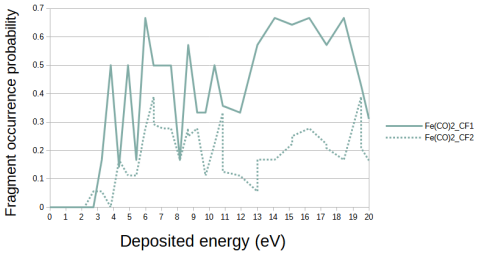

(b) $Fe(CO)_2$

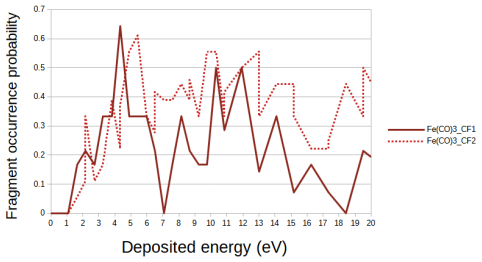

(c) $Fe(CO)_3$

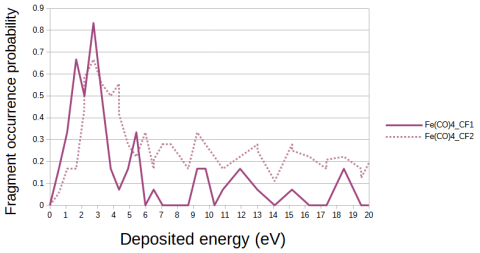

(d) $Fe(CO)_4$

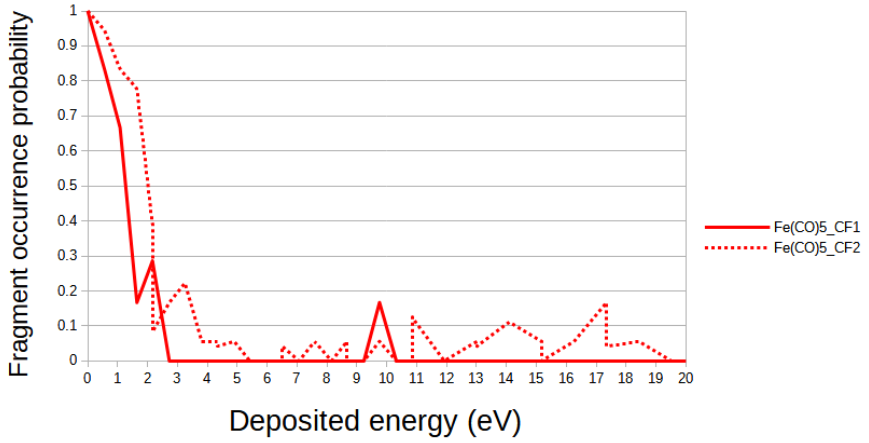

(e) $Fe(CO)_5$

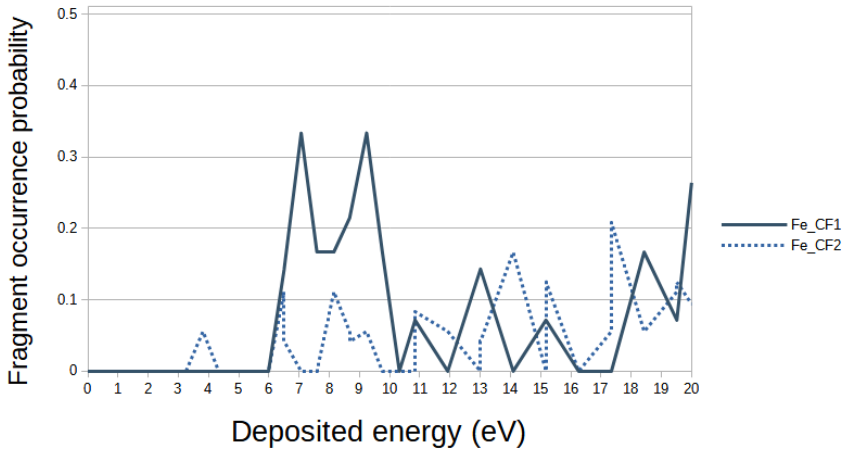

(f) Fe

Figure 3.4: Differences between deposing energy on particular Fe and CF1/CF2 type of bond

are fluctuations of some degree for some channels (but again, statistically looking - they don't appear to be very relevant). Therefore we can assume, that these processes occur independently on the Fe-CF type of bond ionized and dissociated, regardless of being either Fe-CF1 or Fe-CF2.

So far we have confirmed the correctness of our simulation model by comparing the appearance energies with the gas-phase experiment of Lacko (Figure 3.1). I also statistically derived regions of appearance of particular fragment. Although this was important, useful and brought us insight into what is happening on the micro scale, it is a poor representation of FEBID conditions. Model of a molecule floating above the surface is applicable only until we arrive close to the surface of a substrate. A surface is a completely different system, therefore a different model should be taken into account. There are no longer molecules of the same type floating one next to each other, rather the molecule is in contact with either the surface, or with other molecules of already deposited material. A model closely related to that of Lengyel [23] will be utilized.

3.2 Dissociative ionization of iron pentacarbonyl inside argon cluster

Now let us analyse the second system, a $Fe(CO)_5$ molecule embedded into argon cluster (Figure 3.5). I first simulated the pick-up process itself by which the mixed clusters were produced experimentally. Since there is no microscopic evidence of the molecule being on the surface of the cluster (although several works suggest so, [23] and [24]), three different orientations were included in the simulation. In the Figure 3.5, we can see the collision which has been done between centers of mass of both collision partners. Two other inputs for my situation were done by picking up the $Fe(CO)_5$ molecule on a more latteral side of the argon cluster, so that some portion of energy was converted into the rotation of the system, rather than into penetration into higher depth. This way I was able to represent both scenarios - $Fe(CO)_5$ molecule being on top of the cluster, or being embedded deep inside.

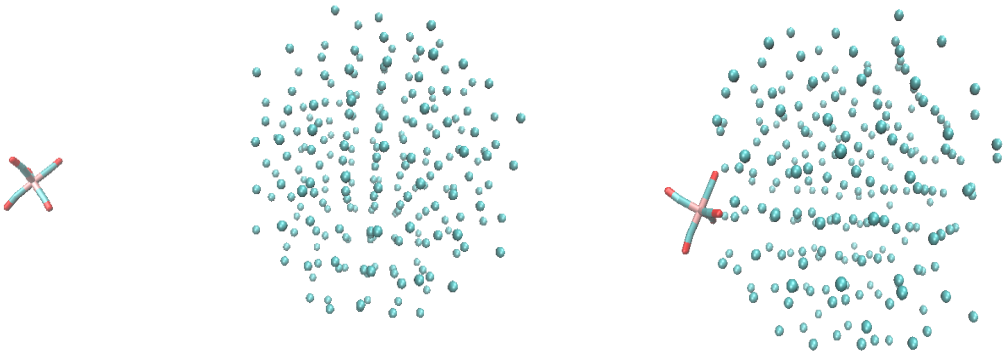

(a) input orientation

(b) moment of collision

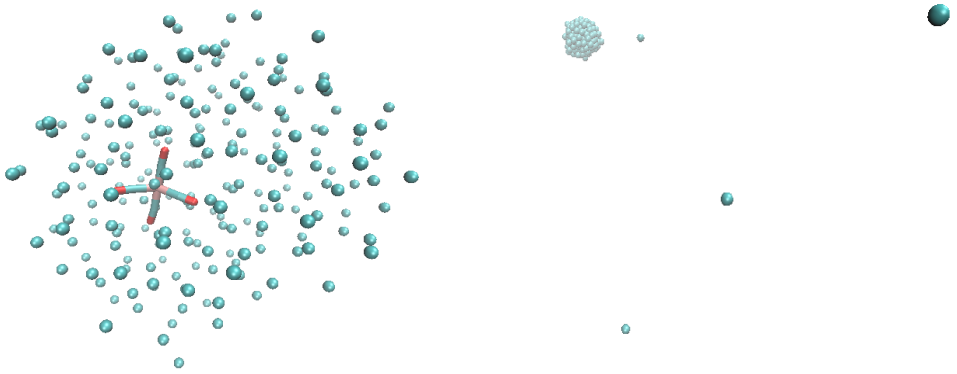

(c) molecule dug into the cluster

(d) thermal evaporation of argon atoms from the cluster

Figure 3.5: Collision of a $Fe(CO)_5$ molecule with argon cluster

Figure 3.6 shows us that even though the collision was performed in a completely different manner (once between the centers of the mass for both systems, once the $Fe(CO)_5$ molecule hit the cluster more lateral from the center, once the pickup process was done due to long range force interaction, not by a direct hit), after thermal cooling and overall thermalization, all of the starting points appear to be very similar. Therefore, we expect the particular results from these three types of inputs of the simulations to be roughly the same.

Now let us take a look, to what extent the cluster affected the dissociation process of the $Fe(CO)_5$ molecule. Experimentally measured values of the appearance energies can be found in table 3.1. In the column marked AE1 are the appearance energies of the fragments in the gas phase, while AE2 stands for appearance energies of these fragments embedded in the argon clusters. As we can see from those values, all of the experimentally measured appearance energies on the argon cluster are located close together.

This fact is depicted in the figure 3.7, along with the values of appearance energies obtained

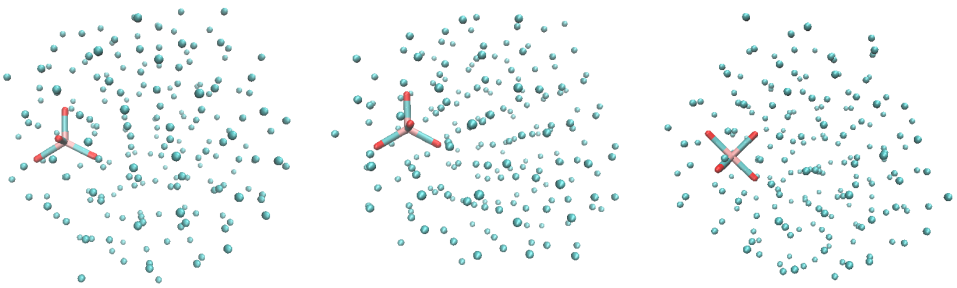

(a) central collision

(b) orbital pickup

(c) lateral collision

Figure 3.6: Collision of a $Fe(CO)_5$ molecule with argon cluster

Cation fragment:	AE1 (eV)	AE2 (eV)
Fe(CO)	12.8	14.8
Fe(CO)2	11.7	14.5
Fe(CO)3	9.7	15
Fe(CO)4	9	14.5
Fe(CO)5	8.3	13.6

Table 3.1: Values of the appearance energies for particular fragments (±0.4 eV) acquired from the work of Lengyel [23]. In the column marked AE1 are the appearance energies of the fragments in the gas phase, while AE2 stands for appearance energies of these fragments embedded in the argon clusters

by our simulations. Just as a reminder I note that ionization energy of the $Fe(CO)_5{}^+$ molecule (AE1, last line) was subtracted from the ionization energy of the $Fe(CO)_5{}^+$ on the cluster (AE2, last line), such that the deposited energy into cation is plotted on the x-axis in the Figure 3.7.

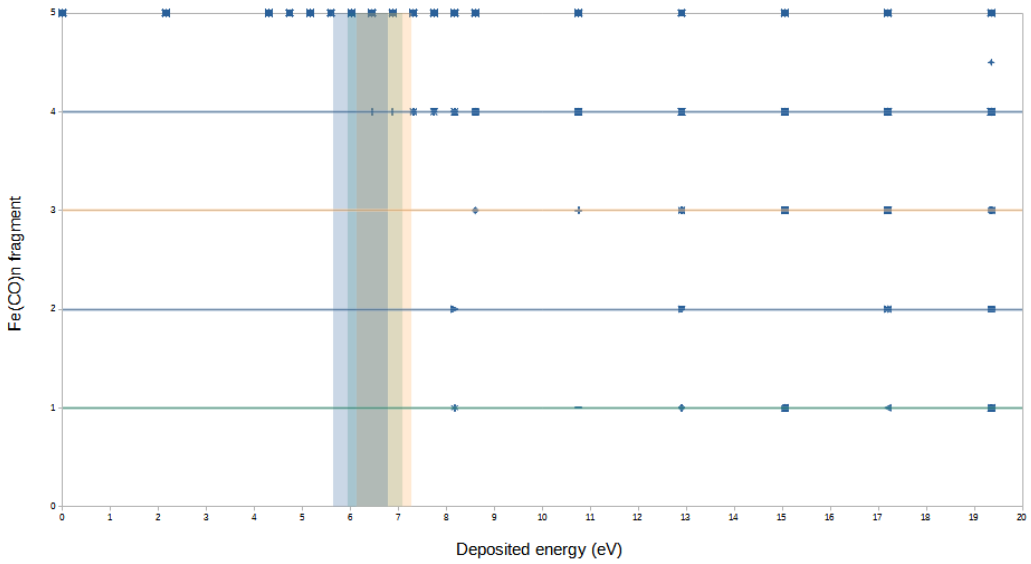

Figure 3.7: Appearance energies of various $Fe(CO)_n{}^+$ ions located inside the argon cluster. Note that in the region around 6.4 eV the experimental appearance energies overlap. For this purpose, a color scheme is introduced with: blue = $Fe(CO)_4{}^+$ and $Fe(CO)_2{}^+$ cations at energy 6.2 eV; yellow = $Fe(CO)_3{}^+$ cation at 6.7 eV and green = $Fe(CO)^+$ at 6.5 eV

By looking at Figure 3.7, one may ask why the values of appearance energies for the sole molecule (figure 3.1) came to much better agreement than the values of the appearance energies obtained in a cluster system. There, only the values for $Fe(CO)_4$ fragment are in agreement with the experiment. As an explanation, I will use the following chart. Out of almost 3000

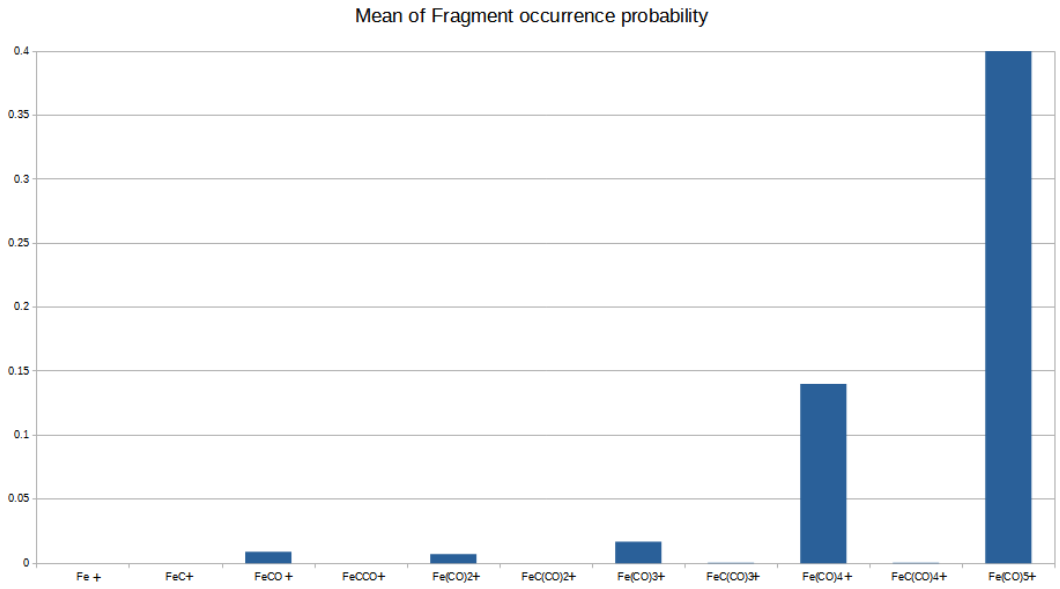

Figure 3.8: Total ratio of the products created from the simulation

simulations, in a simulated time of 25 ps, only a small fraction of the systems dissociated in the described process (ca 20%). Out of this fraction, vast majority of the fragments that were created is $Fe(CO)_4{}^+$. Therefore the comparably small number of the remaining fragments can be a possible answer to why the appearance energies in the Figure 3.7 did not meet the values from the experiment. Simply it should be just a matter of statistics - by creating either more simulations, or increasing the time of the simulations, simulation would produce more of the other fragments than $Fe(CO)_4{}^+$, and therefore match the experiment more accurately.

However, something else can play role in this disagreement. Lengyel et al. [23] suggested that instead of the electron ionizing the $Fe(CO)_5$ molecule directly, electron first ionizes the argon, which transfers the charge into the $Fe(CO)_5$ molecule. Such an effect is not accounted for in the present work.

Total numbers of how many simulations ended up in particular fragmentation is a useful information, but we would like to also see the profiles of the distributions over the energy regions.

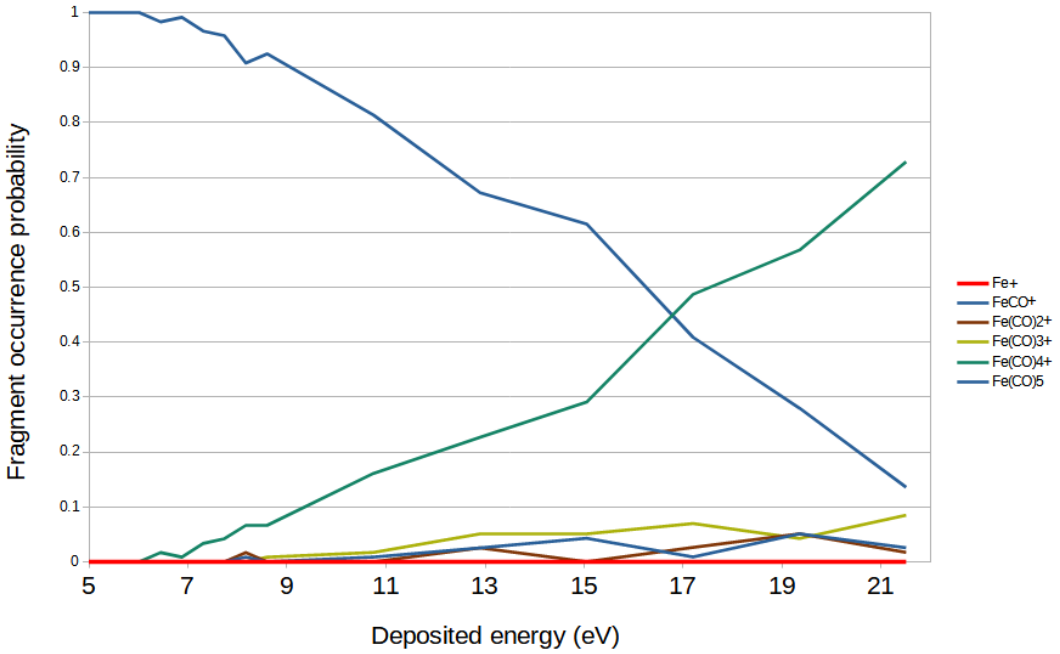

Figure 3.9: Fragment occurrence probability over deposited energy

Comparing Figure 3.9 with 3.2 or 3.3 - we can see that embedding $Fe(CO)_5$ inside the argon cluster causes that the intact $Fe(CO)_5{}^+$ is maintained over much broader region of internal energies. Also the region for the appearance of $Fe(CO)_4{}^+$ fragment is broadening, while the possibility to create any other type of fragment is reduced down to almost none. This is an excellent agreement with the experiment of Lengyel [23], who reported strong ligand stabilization. Both the experiment of Lengyel [23] and my simulations show that the creation of a pure iron product is not present. Also the experiment did not notice fragmentation of the bond between carbon and oxygen, while in my simulation only two such events occured out of almost 3000 simulations.

Let us now focus on the differences caused by the different pick-up processes mentioned earlier. Although the collisions could have created different sets of input orientations, the differences were lost during the thermalization process as was shown in the Figure 3.6. This effect of "degeneration" of the input orientations should be also visible in simulation results. Figure 3.10 is clearly showing us, that these differences were minimized in terms of creating fragments and dissociation of the molecule ligands. Although there are some small deviations visible between these three input (central, orbital, lateral) orientations in terms of particular fragments being formed with a different probability over these three orientations, these differences are very small and therefore statistically insignificant.

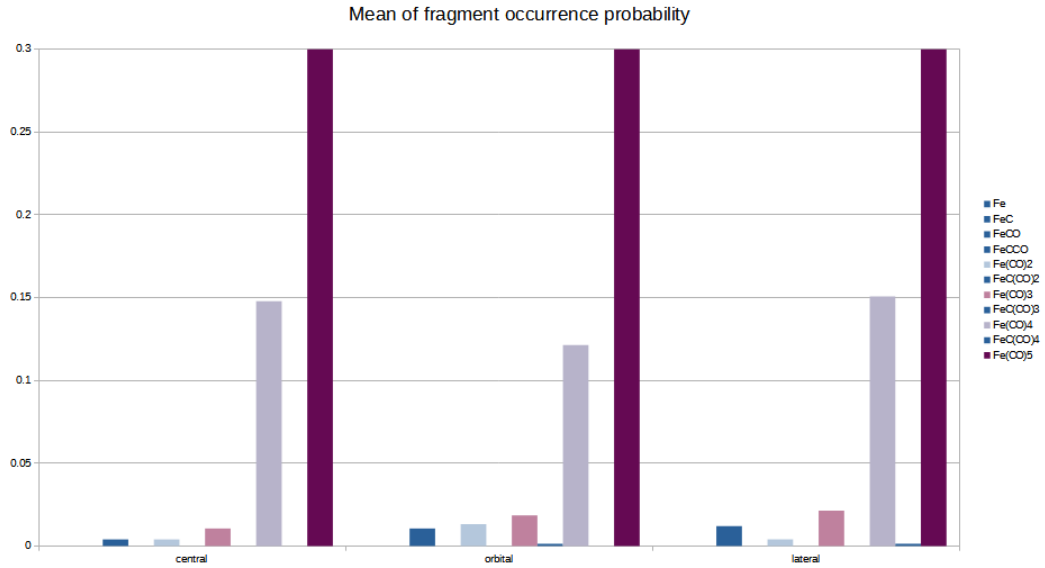

Figure 3.10: Fragment occurrence over total performed simulations

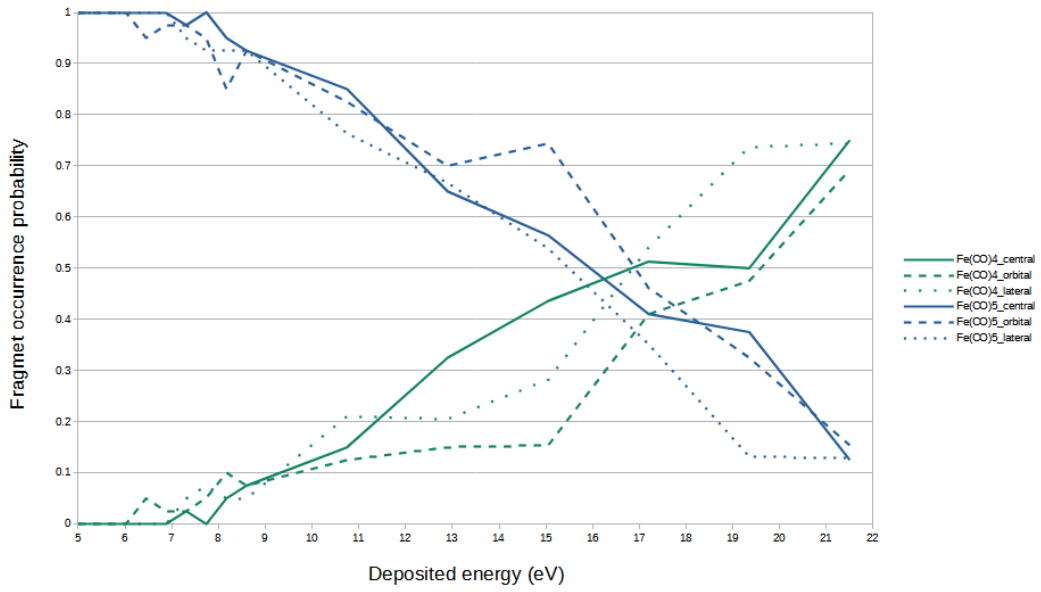

Figure 3.11: Fragment occurrence for clusters created by different pick-up processes

As mentioned before, Figure 3.10 suggests that these three different collisions scenarios ended up in practically equal systems. Also as can be seen in Figure 3.11, there are no major shifts in dissociation regions in terms of its energy threshold, neither in its magnitude. This shows us that these three systems can be considered equal and that the pick-up process does not play a major role in the deviations (or variants) that could appear in the dissociation process.

Last part of analysis comes from the same idea that was discussed around Figure 3.4. Since axial and equatorial CO ligands form a bond with iron with a different dissociation energy, one can analyze, whether this fact plays any role in the dissociation process created by energy transfer to the particular bond. As we could see in Figure 3.4, there were some small differences if we deposited the energy into CF1 (axial) and CF2 (equatorial) type of bond, however they were not so significant, that we could make any interesting outcomes from it.

In the system of molecule embedded in an argon cluster, judging from Figure 3.12, this effect is dramatic. Even though the difference between dissociation energies between i) axial ligand and iron and ii) equatorial ligand and iron is only 0.5 eV, the shift that occurred in

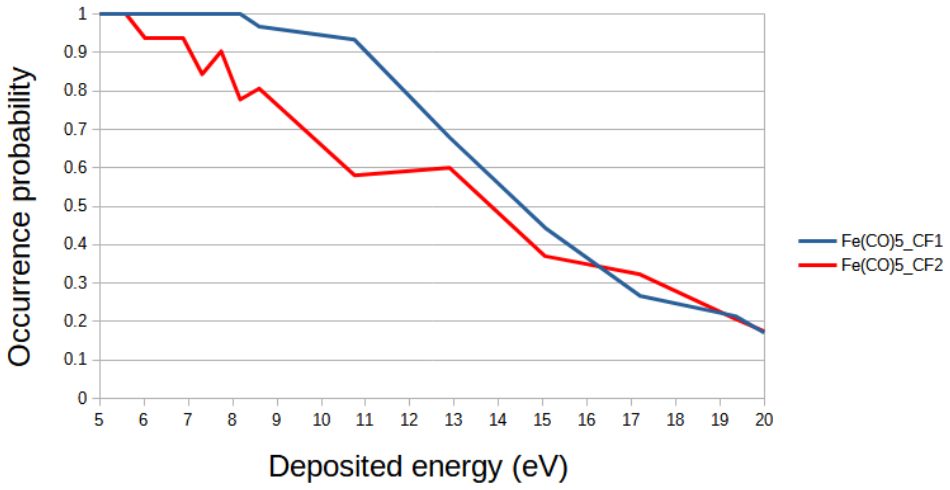

(a) $Fe(CO)_5{}^+$ fragmentation pattern differences based on a different dissociation energy

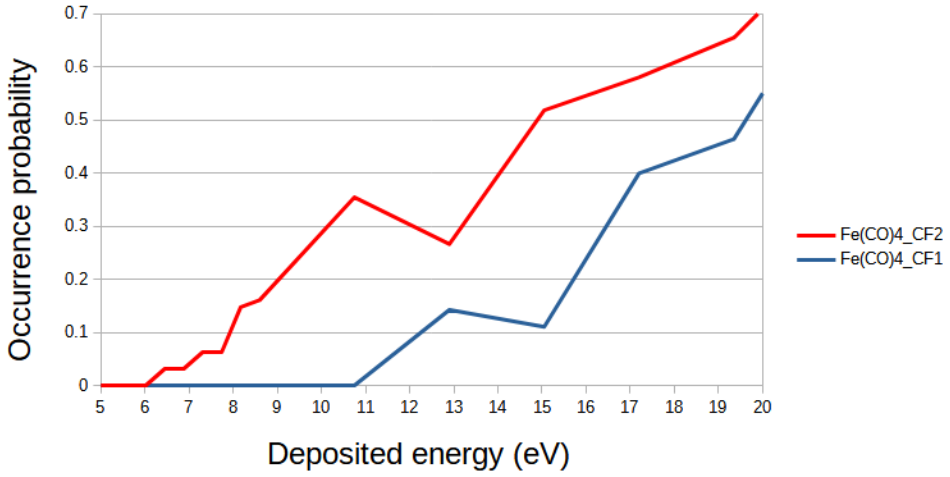

(b) $Fe(CO)_4{}^+$ fragmentation pattern differences based on a different dissociation energy

Figure 3.12

the appearance energies is almost 10 times larger. This means that while the molecule tends to maintain its dissociation pattern proportional to the chemical properties, adding an argon cluster around it creates an environment, where such difference (0.5 eV) suddenly distinguishes the regions significantly. In the isolated molecule, the vast majority of observed dissociation eventswas due IVR. However, on cluster, the IVR process is 'cooled down' by argon, and such dissociation of the cation is not happening. The majority of the single FE-C bond cleavage is prompt. This prompt process will be strongly dependent on the bond strength, hence the observed difference between CF1 and CF2 bonds.

Such amplification effect can influence FEBID performance of precursors where different ligands are bound to the central atom. The science of such heteroleptic (core atom with different kind of ligands around itself) compounds is still being explored [25].

3.3 Gold core surrounded by argon cluster

We now turn to the third, completely different simulated system. The aim was to explore, if non-covalently bound argon cluster can prevent deposition of gold atoms to a substrate. In this work, gold was used instead of more FEBID common elements because the Lennard-Jones potential (for metal-metal, metal-argon and metal-carbon) is described much more accurate, than for the elements like iron. Lastly, graphene layer was used to simulate the substrate. Let us now compare a broad range of possible scenarios to deduce the necessary parameters for the deposition to be viable. Number of gold atoms varied from 1 to 42 atoms and number of argon atoms was around few thousands. Although this range of parameters is rather broad, we will see that these factors are not so important in the final results part.

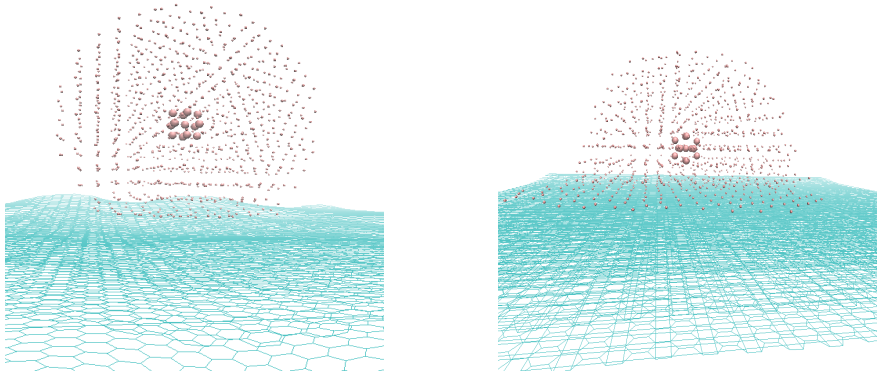

(a) before the drag (b) after the drag (500 ps)

Figure 3.13: cluster of gold and argon dragged to the surface of carbon substrate with van der Waals interactions, temperature of cluster = 0 K, temperature of graphene = 0 K, approaching velocity = 0 m/s

Figure 3.13 indicates, that if both the cluster and the substrate were frozen to 0 K, attractive van der Waals forces would not break the structure of the cluster completely. Although the potential energy of Au-C interaction is stronger (0.044 eV or 1.014 kcal/mol) [26] than the Ar-C (0.028 eV or 0.651 kcal/mol) [27] interaction, if there is a sufficient distance conserved between gold and carbon, as well as sufficient layer of argon cluster preserved above the gold core - the gold does not come to the surface of the carbon substrate.

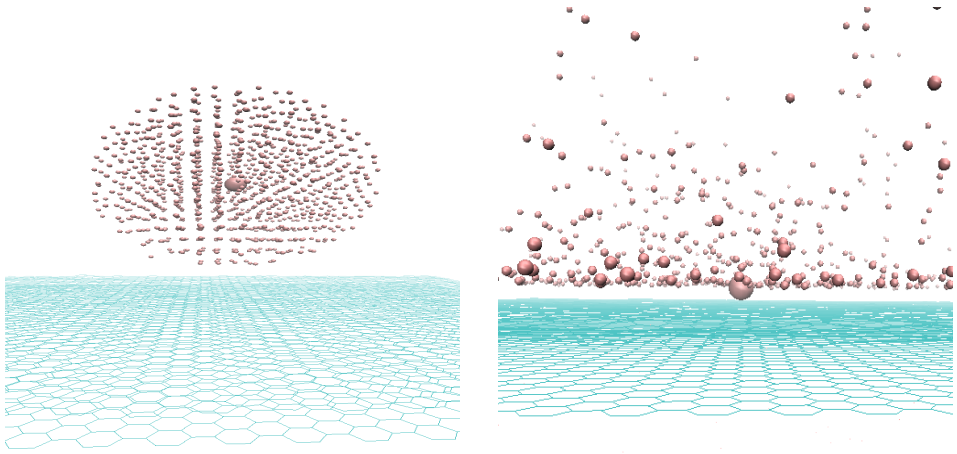

(a) before the landing

(b) shortly after the landing

Figure 3.14: cluster of gold and argon approaching the carbon substrate in typical parameters of laboratory setup

Figure 3.14 is performed with traditional parameters - substrate is 300 K hot, argon cluster has its initial temperature of 40 K and travels with a velocity of 490 m/s, just as in experiments of Lengyel et al. [23]. We can clearly observe, that even without reaching a long time of simulation, with only one atom of gold and cluster consisting of around 950 atoms of argon, this environment tends to break the cluster instantly, causing the gold atom to stick to the surface of the carbon substrate. This certainly means, that special measures need to be taken into account to prevent the ”explosion” of the cluster - both cooling the substrate, and slowing the velocity of approach.

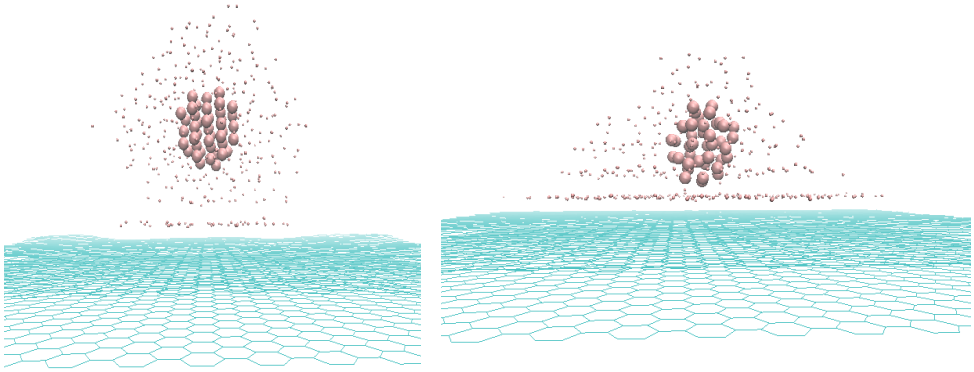

(a) before the landing

(b) after the landing

Figure 3.15: cluster of gold and argon approaching the carbon substrate, both systems cooled to 40 K

In the figure 3.15 it is visible that appropriating the temperature to the point of crystallization of the argon, even after 500 ps of the simulation run, it holds the gold core separated from the surface. Although the layer is thin, and no approaching velocity other than the one caused by van der Waals attraction was added, this observation reveals that such system can be observed in specifically set conditions

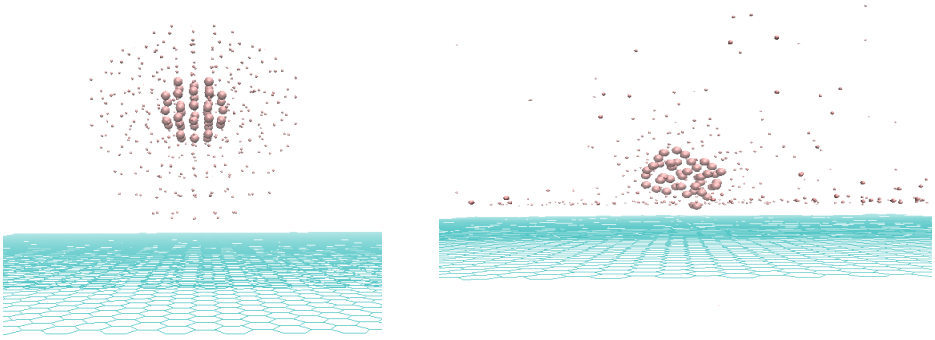

(a) before the landing

(b) after the landing

Figure 3.16: cluster of gold and argon approaching the carbon substrate, both systems cooled to 40 K, with approaching velocity of 12 m/s

As we can see, approaching velocity, or in general - process of putting a cluster on to the surface, is a large task to be resolved. Although such system can exist on the top of the substrate for considerable amount of time, as suggested by figure 3.16, even a velocity of 12 m/s, which is 40 times smaller than an average velocity of an argon cluster beam (described by the work of Lengyel [23]) destroyed the system. Therefore, it might be experimentally challenging to prepare conditions where the argon cluster prevents the deposition of gold. The idea of using argon as ligands in FEBID thus does not appear to be realistic.

Conclusion

After thoroughly inspecting two mentioned systems - 1. $Fe(CO)_5$ in a gaseous phase and 2. $Fe(CO)_5$ embedded in an argon cluster, I have plentiful information to conclude. We have considered two dissociation processes of the isolated $Fe(CO)_5{}^+$ cation. First process is related to the excess energy statistically distributed among atoms, and the second is related to all the excess energy given into Fe-C bond. These considered processes are in good agreement with the experimental data for the case of gas phase $Fe(CO)_5$. Regions of particular -nCO (number of ejected ligands) dissociation were found as a function of the deposited energy. The dissociation process induced by an excess energy given into Fe-C bond has broader regions and overlaps over these regions, than the dissociation process induced by an excess energy statistically distributed among atoms. Probably the most important information FEBID-wise is that the highest pure-iron-creation probability was found to be between 10 and 11 eV with a probability of 32%. Dependence of the ionization regarding a particular type of bond between central atom and ligand (in our case between iron and axial CO ligand, or equatorial CO ligand) was not found in any significant manner, meaning that the different value of dissociation energy does not play a major role in the dissociation process for this system. Therefore there are no visible differences of factor 0.5 eV for an isolated molecule.

Next system which i simulated was $Fe(CO)_5$ embedded in an argon cluster. Since this was not such a straightforward model, more results will be discussed in here. As first - with a given size of the cluster (200 Ar atoms, which was an experimental work [23] average), collision into a different part of the cluster did not result in a different input setup for simulation of the dissociation process. Reason behind this is that the argon cluster somewhat resembles a liquid, which after a long thermalization process from higher temperatures induced by a collision of these two systems ends up surrounding the $Fe(CO)_5$ molecule. This means that the $Fe(CO)_5$ molecule practically can not end up in a conformation, where some of the ligands are pointing out of the system and are not surrounded by this argon cluster. What we observed next is the fact, that both experiment and a simulation observed a shift in appearance energies for all the fragments, however our simulation did not agree with the experiment [23], probably because of insufficient sample of simulations (or simulation times) and maybe even more important - because of the charge transfer process from the argon cluster into the $Fe(CO)_5$ molecule. Instead of the electron ionizing the $Fe(CO)_5$ molecule directly, electron first ionizes the argon gas, which transfers the charge into the $Fe(CO)_5$ molecule, as is suggested by Lengyel et al. [23]. However, a few important and interesting conclusions are to be mentioned. 1) In both simulation and experiment, no pure iron cations were observed at the end of dissociation process. 2) argon as a medium dramatically shifts and broadens the regions of the occurrence of particular fragments. 3) Insignificant number of C-O bond breaking was observed in simulations (2 out of 3000), which corresponds to none of the $FeC(CO)_n{}^+ + O$ fragments being measured in the experiment.

Finally, simulation of the landing of the gold embedded in an argon cluster ended up in several observations. First, this problem seems to depend only a little on the cluster and the core size. What seems to matter the most is to keep the surface of the substrate below the melting temperature of the argon cluster (40 K), similarly to the work of Palmer et al. [28], where the surface temperature was kept at 9 K to achieve this effect. Furthermore, injecting the cluster to the surface in a setup similar to the one used in the experiment of Lengyel [23] results in a complete scatter of the argon back from the surface and even when the approaching velocity was set to 12 m/s (compared to experimental 490 m/s), the system immediately broke its original shape and lost its protecting function. Therefore, argon clusters do not prevent deposition of gold. If there was any other way to transfer the cluster into the surface of the substrate without making it collide with the surface, then this argon cluster probably could provide a protection from the unwanted deposition.

Bibliography

[1] I. Utke, P. Hoffmann, J. Melngailis, J. Vacuum Sci. Technol. B 26, **1233** (2008)

[2] Nanofabrication Using Focused Ion and Electron Beams (2012) **17**, Ivo Utke, Stanislav Moshkalev, and Phillip Russell, ISBN: 9780199734214

[3] Lacko, M., Papp, P., Wnorowski, K. et al. Electron-induced ionization and dissociative ionization of iron pentacarbonyl molecules. Eur. Phys. J. D 69, 84 (2015). https://doi.org/10.1140/epjd/e2015-50721-8

[4] R.E. Winters, R.W. Kiser, Negative-Ion Metastable Transitions in Metal Carbonyls Inorg. Chem. 3, 4 (1964)

[5] B.R. Conard, R. Sridhar, Appearance potentials of ion fragments of iron pentacarbonyl Can. J. Chem. 56, 2 (1978)

[6] A. Foffani, S. Pignataro, B. Cantone, F. Grasso, Mass Spectra of Metal Hexacarbonyls* Z. Phys. Chem. (Frankfurt) 45, 78 (1965)

[7] D.R. Bidinosti, N.S. McIntyre, Electron-impact study of some binary metal carbonyls Can. J. Chem. 45, 641 (1967)

[8] G.A. Junk, H.J. Svec, Energetics of the Ionization and Dissociation of Ni(CO)4, Fe(CO)5, Cr(CO)6, Mo(CO)6 and W(CO)6 Z. Naturforsch. B 23, 1 (1968)

[9] P.J. Clements, F.R. Sale, Deposition of iron, nickel and iron-nickel layers from carbonyl vapors Metal. Trans. B 7, 171 (1976)

[10] L.F. Pasteka, T. Rajsky, M. Urban, Toward Understanding the Bonding Character in Complexes of Coinage Metals with Lone-Pair Ligands. CCSD(T) and DFT Computations. The Journal of Physical Chemistry A 2013, 117 (21) , 4472-4485.

[11] Barth, Sven and Huth, Michael and Jungwirth, Felix,
Precursors for direct-write nanofabrication with electrons
J. Mater. Chem. C **8**, 15884-15919 (2020)

[12] M. Gavagnin, H. D. Wanzenboeck, D. Belic, M. M. Shawrav,
A. Persson, K. Gunnarsson, P. Svedlindh and E. Bertagnolli,
Phys. Status Solidi A, 2014, **211**, 368–374.

[13] M. Gavagnin, H. D. Wanzenboeck, D. Belic and E Bertagnolli,
ACS Nano, 2013, **7**, 777–784.

[14] T. Lukasczyk, M. Schirmer, H.-P. Steinruck and H Marbach,
Small, 2008, **4**, 841–846.

[15] G.B.Sushko, I.A. Solov'yov, A.V. Solov'yov, Modeling MesoBioNano systems with MBN Studio made easy, J. Mol. Graph. Model. 88 (2019) 247-260

[16] Solov'yov IA, Yakubovich AV, Nikolaev PV, Volkovets I, Solov'yov AV.
MesoBioNano Explorer–a universal program for multiscale computer simulations of complex molecular structure and dynamics. J Comput Chem. 2012 Nov 15;**33(30)**:2412-39

[17] Ilia A. Solov'yov, Andrey V. Korol, Andrey V. Solov'yov
Multiscale Modeling of Complex Molecular Structure and Dynamics with MBN Explorer
Springer International Publishing AG 2017, 48

[18] L. Verlet, Phys. Rev. **1967**, 159, 98103.

[19] W. H. Press, S. A. Teukolsky, W. T. Vetterling, B. P. Flannery, Numerical Recipes 3rd Edition: The Art of Scientific Computing; Cambridge University Press, Cambridge, UK, **2007**.

[20] L. Landau, E. Lifshitz, Statistical Physics; Elsevier, Butterworth- Heinemann: Oxford, **1980**.

[21] Gennady B. Sushko, Ilia A. Solov'yov, Alexey V. Verkhovtsev, Sergey N. Volkov and Andrey V. Solov'yov Studying chemical reactions in biological systems with MBN Explorer: implementation of molecular mechanics with dynamical topology Eur. Phys. J. D (2016) 70: 12

[22] Pablo de Vera, Alexey Verkhovtsev, Gennady Sushko, and Andrey V. Solov'yov Reactive molecular dynamics simulations of organometallic compound W(CO)6 fragmentation Eur. Phys. J. D (2019) 73: 215

[23] Ligand Stabilization and Charge Transfer in Dissociative Ionization of Fe(CO)5 Aggregates J. Lengyel, J. Fedor, and M. Fárník The Journal of Physical Chemistry C 2016 120 (31), 17810-17816

[24] J. Lengyel, J. Kočišek, M. Fárník, and J. Fedor Self-Scavenging of Electrons in Fe(CO)5 Aggregates Deposited on Argon Nanoparticles The Journal of Physical Chemistry C 2016 120 (13), 7397-7402 DOI: 10.1021/acs.jpcc.6b00901

[25] Focused Electron Beam-Induced Deposition and Post-Growth Purification Using the Heteroleptic Ru Complex (η_3-C_3H_5)Ru(CO)$_3$Br
Jakub Jurczyk, Christopher R. Brewer, Olivia M. Hawkins, Mikhail N. Polyakov, Czeslaw Kapusta, Lisa McElwee-White, and Ivo Utke
ACS Applied Materials and Interfaces 2019 11 (31), 28164-28171 DOI: 10.1021/acsami.9b07634

[26] Soft landing of metal clusters on graphite: a molecular dynamics study
Alexey V. Verkhovtsev, Yury Erofeev and Andrey V. Solov'yov
Eur. Phys. J. D (2020) 74: 205

[27] Ab initio and analytic intermolecular potentials for Ar–CH3OH.
Tasić, U., Alexeev, Y., Vayner, G., Crawford, T. D., Windus, T. L., Hase,
W. L. (2006). Phys. Chem. Chem. Phys., 8(40), 4678–4684. doi:10.1039/b609743j

[28] Spadaro, M., Cao, L., Terry, W., Balog, R., Yin, F., Palmer, R.
Spadaro, Maria Chiara Cao, Lu Terry, William Balog, Richard Yin, Feng Palmer, Richard. (2020). Size control of Au nanoparticles from the scalable and solvent-free matrix assembly cluster source. Journal of Nanoparticle Research. 22. 10.1007/s11051-020-04869-9.

[29] R. Essajai, I. Tabtab, A. Mzerd, O. Mounkachi, N. Hassanain, M. Qjani, Molecular dynamics study of thermal properties of nanofluids composed of one-dimensional (1-D) network of interconnected gold nanoparticles, Results in Physics, Volume 15, 2019, 102576, ISSN 2211-3797, https://doi.org/10.1016/j.rinp.2019.102576.

List of Figures

List of Tables

List of Abbreviations

A. Attachments

A.1 First Attachment